Surface Science 754 (2025) 122677

Contents lists available at ScienceDirect

Surface Science

journal homepage: www.elsevier.com/locate/susc

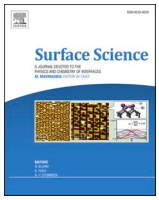

The chemistry of bimetallic surfaces – Evolution of an atomic-scale picture

R. Jürgen Behm *, Axel Groß

Institute of Theoretical Chemistry, Ulm University, Oberberghof 7, Ulm 89081, Germany

ARTICLE INFO

Keywords:
Bimetallic surfaces
Bimetallic catalysts
Adsorption
Catalytic surface reaction
Structure-reactivity concepts

ABSTRACT

In this contribution, we will review the concepts and principles used to characterize and discuss the structure, stability, adsorption properties and catalytic reactivity of bimetallic surfaces in an atomic-scale picture. Starting from early stages, we will emphasize recent experimental and theoretical findings that resulted in a rapidly improving atomic-scale understanding of adsorption and catalytic surface reactions on these surfaces. While examples are often taken from our own work, the resulting insights are of general validity.

1. Introduction

Bimetallic surfaces and catalysts and their chemical and catalytic properties have attracted considerable interest over the last several decades, both from fundamental reasons, but in particular because of their attractive catalytic properties, which were found to often exceed the performance of their constituents in terms of activity, selectivity and stability [1–6]. The improved catalytic performance was attributed to an interplay of a number of different effects such as geometric ensemble effects, electronic ligand effects and electronic strain effects, where the first describes the influence of the size/configuration of active surface ensembles [7–10]. Electronic ligand effects describe the effect of electronic modifications of the active site by different neighboring surface atoms [9,11–14]. These as well as strain effects, which reflect the effect of lattice distortions as compared to the natural lattice of the respective surface layer on the electronic structure [15], can lead to changes in the adsorption energy of reactants and thus to significant modifications in the reaction kinetics [16–18]. Finally, site-blocking effects, which reduce the number of active sites, have to be considered as well [19–21]. Initially, these different effects were mainly concluded from changes in the catalytic activity upon varying the concentration of the respective components in bimetallic catalysts [1,3,22–24] and polycrystalline bimetallic films [3,4,11,25]. More detailed, atomic-scale insights were gained from Surface Science type model studies on structurally well-defined, single-crystalline bimetallic surfaces [6,14,26–28], which started in the late 1970s [19,29–33]. Due to the rather well defined nature of these model surfaces, these studies allowed to more directly derive correlations between structural and electronic properties on the one hand and chemisorption and catalytic properties on the other hand. Nevertheless, despite the considerable progress in the atomic scale understanding of the chemistry of bimetallic surfaces, also these studies were limited in their predictive power because of missing information on structural and electronic details such as the defect structure, atom distribution in bimetallic surface layers etc. This information became accessible only with the advent of modern high-resolution spectroscopies and microscopies, in particular high-resolution scanning tunneling microscopy (STM) and, equally important, the development and application of powerful theoretical methods, in combination with the increasing knowledge in the reproducible preparation of structurally well-defined model surfaces / systems.

In this contribution, we will review the concepts used to discuss the structure, stability, adsorption properties and catalytic reactivity of bimetallic surfaces, with special emphasis on recent experimental and theoretical findings. While examples are often taken from our own work, the resulting insights are of general validity.

2. Bimetallic surfaces

2.1. Definition of bimetallic surfaces

The term ‘bimetallic surfaces’ refers to surfaces, whose surface region - not necessarily only the topmost atomic layer – consists of two metal components, whose physical and chemical properties are determined by these two components. This distinguishes them from so-called high entropy alloys, which according to their definition consist of five and more principal components with concentrations between 5 and 30 % [34]. Focusing on the distribution of the metal components in the surface region, this includes a number of different structural

* Corresponding author.
E-mail address: juergen.behm@uni-ulm.de (R.J. Behm).

https://doi.org/10.1016/j.susc.2024.122677
Received 26 September 2024; Received in revised form 19 November 2024; Accepted 2 December 2024
Available online 3 December 2024

configurations. On the one hand, there are surfaces where the topmost layer(s) are intermixed, such as surfaces of metal bulk alloys or of two-dimensional (2D) alloy films of a monolayer (monolayer surface alloys) or a few layers thickness, supported on a monometallic metal support [35]. On the other hand, they include surfaces formed by an ultrathin film of one or more atomic layers thickness of metal A, which is deposited on a (metallic) support formed by a different metal B, where the surface properties of the film are modified by the presence of the support. A special case are near surface alloys (NSAs), which were defined as alloys where a solute metal is present near the surface of a host metal in concentrations different from the bulk [36]. Considering structural properties, pseudomorphic films refer to films that continue the structure of the single-crystalline support, while in other cases, where the misfit between the natural lattices of support and deposit is too large, structural changes occur mostly in the deposit layer.

Thermodynamically stable (see below) monometallic films (A) on a metal support (B) can be formed if the metal A does not form solid solutions in the bulk of B. In many cases, however, the confinement to the top layer(s) is reached by kinetic limitations, which kinetically stabilize the film against bulk dissolution. The same is true also for surface alloys on top of a monometallic substrate. For surfaces of bulk alloys, the composition of the surface region may differ significantly from that of the bulk composition, depending on the experimental conditions. Here it is important to note that essentially all of these model film systems with typically $> 10^6$ metal layers in the support and up to a few atomic layers in the film are only metastable at temperatures reached during preparation of such model system, due to the extreme dilution. Intermixing is thermodynamically favored for entropic reasons, and in most cases the films are only stabilized by kinetic limitations against bulk dissolution

Changing from massive bulk samples to metal nanoparticles, the different types of film systems are often denoted as core-shell systems, where core and shell consist of different mono- or bimetallic phases.

In the following, we will focus on the structural, electronic, chemical and catalytic properties of structurally well-defined, single-crystalline bimetallic model surfaces, where compared to mostly polycrystalline technical surfaces the variety of different surface sites is significantly lower. This allows a quantitative determination and evaluation of the abundance of different structural elements (see next section), which is mandatory for an unambiguous interpretation of the results obtained from adsorption and catalysis studies.

2.2. Structure and morphology of bimetallic surfaces

The (crystallographic) structure of smooth bimetallic surfaces consisting of a support and a mono- or bimetallic surface region is generally determined by a balance between strain energy and interface energy. (Note that this neglects small variations in the surface energy of the deposit upon structural modifications.) The first parameter defines the energy costs for expanding / compressing the deposit lattice along the surface from its bulk value to the final lattice, while the interface energy describes the energy gained / lost upon interface formation compared to the interaction with a bulk substrate of the deposit material. Obviously, the strain energy depends on the film thickness, and increases with increasing number of atomic layers. The interface energy, on the other hand, does not vary with film thickness, at least not to first order. It depends on the misfit between substrate and deposit lattice and the specific nature of support and deposit, and is generally minimized for a pseudomorphic structure with no apparent misfit between support and actual deposit lattice. As a result, there is a driving force for ultrathin deposit layers to restructure with increasing thickness and finally approach and adopt the bulk structure of the deposit, e.g., by the formation of misfit dislocations [37–41]. This is often discussed as one of the origins for the change from layer-by-layer growth to 3D island formation during Stranski-Krastanov growth [42–44]. Excellent overviews on these aspects are given in ref. [45].

Up to the late 1980′s, the surface structure was mainly derived from inspection of low energy electron diffraction (LEED) patterns, which gave access to the structure of the surface unit cell and to the defect density. Differences in the support and film lattices resulted in the emergence of additional diffraction spots, in addition to the support related reflections [29,30,41,46]. Furthermore, the defect density in the deposit films, including also steps and island formation, was derived from spot splitting and the width of the additional diffraction spots [46]. Similar information was obtained also from X-ray scattering [47]. A more local picture, up to the quantitative determination of specific atomic structures, was possible with the advent and introduction of scanning tunneling microscopy (STM). High resolution imaging, up to atomic resolution [48–50] and even with chemical contrast between different metals [51–53], allowed the identification and quantification of characteristic structural elements such as misfit dislocations [39,40, 49,54], and even to quantify the two-dimensional distribution of surface atoms in bimetallic surface layers [55–58]. Information on the nature and abundance of different adsorption sites was also obtained by spectroscopic titration of different adsorption sites, using suitable adsorbates such as CO [59–62].

STM imaging also provided detailed information on the nature and abundance of the structural defects created during preparation of the bimetallic model surfaces, which is mostly done by vapor deposition of the respective metal(s) and subsequent annealing. In many if not most cases, the resulting surface morphology is determined by kinetic limitations rather than by the thermodynamic system properties (see Section 2.1). Examples of the resulting structures of bimetallic surfaces, as imaged by STM, are shown in Fig. 1. Depending on the deposition and subsequent annealing temperatures, this may result in highly defective surfaces, with large numbers of different island structures, if the temperature is too low to reach the thermodynamically expected smooth form. On the other hand, too high temperatures may result in the onset of surface intermixing, which is not easily detectable or even quantifiable with standard surface techniques. Furthermore, also adsorption or reaction may result in a restructuring of the bimetallic surface, e.g., in a partial de-alloying of the surface layer due to segregation / bulk dissolution [63–65] or, in electrochemistry, due to electrochemical dissolution [66–68]. Also these processes may, however, be hindered or even inhibited by kinetic limitations. Because of the considerable influence of such defects on the adsorption and in particular on the reaction properties, the correct interpretation of the results of adsorption and/or reaction measurements on bimetallic surfaces requires a careful check of the defect structure of the respective surface and changes therein. This is most directly achieved by comparison of representative STM images taken before and after the adsorption / desorption / reaction process.

Focusing on bimetallic PdAg and PtAg surfaces, their structure differs depending on whether these surfaces were fabricated by using Ag (111) as support with Pt (Pd) as deposit or Pt(111) (Pd(111) as support and Ag as deposit material, or whether they represent surfaces of bulk alloys. In the first case, intermixing / surface alloy formation and also bulk dissolution are activated already at rather low temperatures, at room temperature and slightly above, when the noble metals are deposited on Ag(111) [69–74]. This can be rationalized considering that Pt has a significantly higher cohesive energy than Ag. Therefore, one would expect that Pt interacts more strongly also with Ag than Ag with Ag. This provides a considerable driving force for the exchange of a Pt adatom with a Ag surface atom during Pt deposition. In the opposite case, deposition of Ag on a Pt surface, the driving force for such exchange would be much less or non-existent, as the Pt-Pt interaction is stronger than the Pt-Ag interaction. Considering also that according to the Brønsted-Evans-Polanyi principle [75] the kinetic barrier depends strongly on the energy of the final state relative to the initial state, the high stability of a Pt atom embedded in the topmost Ag layer facilitates the exchange of a Pt adatom with a Ag surface atom and thus the intermixing of Pt deposited on Ag as compared to Ag deposition on Pt. Furthermore, for Pd deposition, encapsulation of the Pd islands is observed before the onset of intermixing or bulk diffusion [73]. Hence,

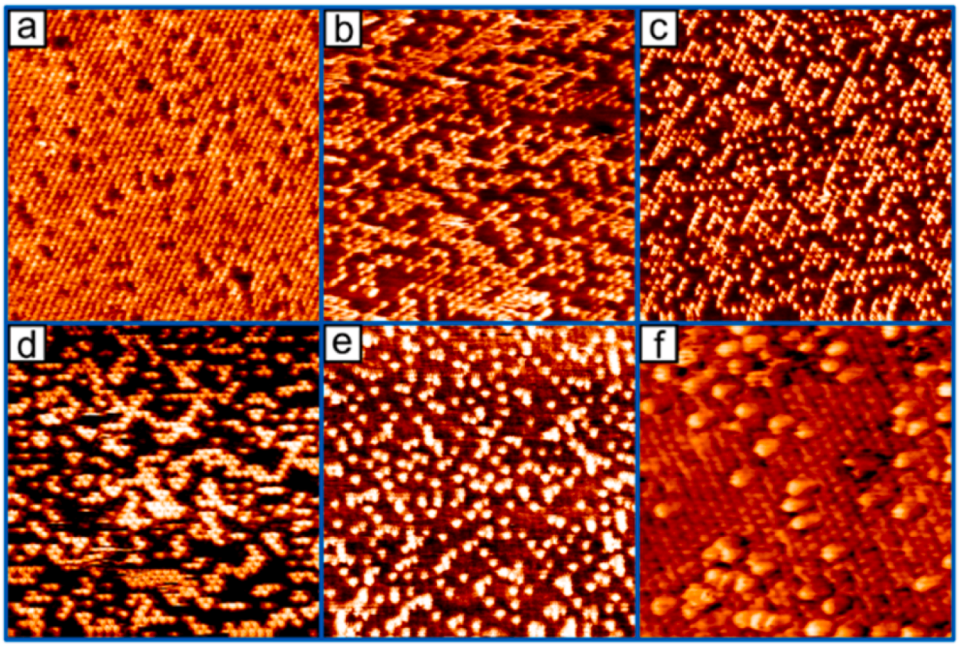

Fig. 1. High resolution STM images showing Pd_xAg_{1-x}/Pd(111) surface alloys with different Ag surface contents (10 nm × 10 nm) after annealing at 800 K for 10 s. (a) 10 % Ag; (b) 35 % Ag; (c) 50 % Ag; (d) 65 % Ag; (e) 76 % Ag; (f) surface originally covered by 1.7 ML of Ag (7.5 nm × 7.5 nm).). Reprinted from Engstfeld et al. [58].

the formation of well-defined, kinetically stabilized monolayer films and surface alloys is not possible under these conditions. This is different when using Pd(111) or Pt(111) as support, where the much higher cohesion energy points to higher kinetic barriers for exchange / surface intermixing and bulk dissolution of Ag. As a result, well-defined Ag films with thicknesses from the submonolayer to a few atomic layers can be produced both on Pd(111) [76–80] and Pt(111) [81,82]. Only upon annealing to ≥ 450 – 500 K (Pd(111)) [58,60,83,84] or ≥ 620 K (Pt (111)) [57,85], surface exchange and intermixing set in, which at these conditions are confined to the topmost layer ('surface confined intermixing') [57,62,85–90]. Dissolution into deeper regions or Ag desorption (PtAg/Pt(111)) set in upon annealing to ≥ 600 K (Ag/Pd(111)) [60] or ≥ 900 – 950 K (Ag/Pt(111)) [81,91]. Thus, there is a considerable temperature range where these bimetallic surfaces are kinetically stabilized and where adsorption or reaction processes may be investigated without modifying the surface structure and composition.

For the surface alloys, the two-dimensional (2D) distribution of the surface atoms is a crucial parameter, as it determines the abundance of different types of adsorption sites. For AB surfaces with large islands of A or B surface areas ('2D phase separation'), the fraction of mixed A_xB_y type sites will be small, while for a random distribution this should be much larger, and it would be even larger for preferential mixing. The resulting 2D distributions and the related short-range order parameters (SROs) [92] were evaluated quantitatively from atomic resolution scanning tunneling microscopy (STM) images with chemical contrast for different surface concentrations of Ag and Pd [58] (see Fig. 1) or Ag and Pt [57]. These distributions and trends therein with increasing Pd or Pt concentration provide a basis for the identification of preferential adsorption and reaction sites (see Sections 3.1 and 3.2). Quantitative statistical evaluation of these images yielded an essentially random distribution of the Pd and Ag surface atoms for the different PdAg/Pd (111) surfaces [58], while for PtAg/Pt(111) systems the data revealed a clear tendency toward 2D phase separation [57,93]. The impact on the adsorption properties will be discussed in Section 3.1.

Finally, the formation of single-atom surface alloys was reported by Maroun et al. for Pd/Au(111) [94] and more recently for Pd/Ag(111) and Pt/Ag(111) by Muir and Trenary [95] and by Patel et al. [70], respectively. These single-atom model catalysts differ from Pd or Pt monomers in PdAg/Pd(111) or PtAg/Pt(111) monolayer surface alloys by the different environment of the active Pd or Pt surface atoms, with Ag neighbors in all directions for the single-atom systems, while in the other case surface Pd or Pt atoms bind to an underlying Pd(111) or Pt (111) support. Furthermore, they differ in their lattice constant. Muir and Trenary observed by IR spectroscopy that upon room temperature deposition of small amounts of Pd, up to approximately 0.002 monolayers, Pd/Ag(111) forms a single-atom alloy, which was demonstrated by CO titration [95]. Saturation of the surface with CO led to the formation of CO adsorbed at Pd atop sites, but not at Pd_2 bridge sites, indicating that the Pd atoms are isolated from each other. These Pd monomers are not stable with respect to subsurface alloy formation or Pd diffusion into the bulk, as indicated by the decay of the related IR band upon annealing the surface to 350 K and more (complete disappearance after annealing the surface to 450 K). For Pt/Ag(111), formation of Pt monomers was concluded from the presence of a lower-temperature CO desorption peak at 380 K in temperature programmed desorption (TPD) spectra, which were recorded after Pt deposition at 380 K and saturation of the surface with CO at 90 K [70]. This peak, which was observed up to rather high Pt coverages (> 0.22 monolayers), was associated with a weakly bound CO species on surface Pt monomers (see also the discussion in Section 3.1).

2.3. *Electronic properties of bimetallic surfaces*

Initially, the electron characteristics of solids had been discussed and proposed as a guide to their catalytic activity [2,96–100]. More specifically, the activity of a metal was considered to depend on the values of the electronic work function, the electronic density of states (DOS) at the Fermi energy and the gradient therein [97,99]. For a series of binary solid solutions containing one of the group 8 elements (Ni, Pd or Pt) together with one of the group I elements (Cu, Ag or Au) or the binary alloys of iron, cobalt and nickel, the efficacy in multiple bond saturation or in dehydrogenation was found to depend largely on the number and the characteristics of the holes in the d-bands of the alloys [2,22,98]. Hence, the influence of the electronic properties of a catalyst on its activity was discussed in a non-local picture, by relating it to different bulk electronic properties [2,101]. Modifications in the catalytic activity of a

metal catalyst by addition of a second metal were explained by donation or removal of electrons to/from the dominant component, comparable to the concept of Hume-Rothery phases [102]. For the theoretical description, effective Hamiltonians such as in the Newns-Anderson model [103] were used.

Later studies distinguished between bulk and surface electronic properties, considering that the catalytic properties should be mainly related to the surface electronic structure [104,105], in addition to geometric effects. Furthermore, the focus changed to a local picture, using the local density of states (LDOS) on the respective surface atoms [106]. This is particularly important for bimetallic surfaces, where the electronic properties of the two different types of surface atoms should be different. But similar effects are expected also for structural defects, as the electronic properties of a step edge atom are different from those of terrace surface atoms.

Therefore, theoretical as well as experimental studies have typically concentrated on the local density of states of surface metal atoms and how it is modified by their immediate environment [17,107]. Motivated by the success of the frontier orbital concept, the local density of states at the Fermi energy has been correlated with the reactivity of metal surfaces [104–106]. However, metal alloy surfaces such as $Cu_3Pt(111)$ exhibit a very low density of states at the Fermi level, but are still rather reactive [108]. Hence, instead the position of the d-band center and in particular the shift of the d-band center have been considered in order to understand reactivity trends at metal surfaces, as within the d-band model changes in the reactivity of a transition metal atom are directly related to shifts in its local d-band center [108]. The d-band model predicts a linear relationship between the d-band center shift and the change in the interaction strength [109]. The lower the d-band center is below the Fermi energy, the weaker the interaction with adsorbates becomes, i.e., the reactivity of these metal atoms with respect to adsorption decreases. The physical origin of possible changes of the d-band and its center for a late d-band metal upon modifying the structure and/or composition of the metal surface is illustrated in Fig. 2.

In this figure, the density of states of a late d-band metal with a not completely filled d-band is illustrated. As the name indicates, the d-band model focuses on the d-band density of states. Of course, the s-electrons of a d-band metal also contribute significantly to the interaction with reactants, however, their contribution is rather similar for all dd-band metals and surface structures [108]. Hence, their contribution is disregarded in the comparison between different d-band metals and/or surface structures. Upon increasing the d-band width symmetrically about the d-band center for a more than half-filled d-band, e.g., due to compressive strain or higher coordination, the portion of the d-band that is located above the Fermi energy becomes larger, i.e., the occupation of the d-band would decrease. This change of the band width is illustrated in Fig. 2b, where otherwise the d-band center was kept constant with respect to panel a). In order to keep the number of occupied d-electrons constant, the d-band has to shift down (see Fig. 2c). It is important to note that for metals with a completely filled d-band or a less than half filled dd-band the situation is different. In the former case broadening or compression of the d-band would not cause any shift of the d-band and its center, while for early transition metals a broadening of the d-band should lead to an up-shift of the d-band center. Practically, however, the situation depicted in Fig. 2 is dominant, as catalysts typically involve late transition metals.

In the d-band model, the whole distribution of the d-band states is represented by its center, which mathematically corresponds to the first moment of the distribution of the d-band densities of states. However, using just the d-band center as a descriptor for the surface reactivity also yielded some outliers [110], which motivated theoretical studies [110, 111] to investigate the influence of the d-band shape, represented by higher moments of the d-band, on the interaction strength with adsorbates. First of all, these two studies confirmed that the position of the d-band center indeed better reflects trends in the adsorption energies, in particular for alloy surfaces, than the d-band width W_d, which corresponds to the second moment of the distribution. However, a slight improvement for some metal systems was reached, when instead of the d-band center ε_d the upper edge of the d-band $\varepsilon_d + W_d/2$ was chosen as the descriptor. However, because of its computational simplicity, the original d-band model with its pure focus on the d-band center is still predominantly used to understand trends in surface reactivity.

We are now focusing on one particular metal atom in the surface of a bimetallic surface, and thus on the local density of states (LDOS) at that atom. Imagine that the surface layer is under compressive strain. This can, for example, be achieved by the pseudomorphic growth of a metal layer on a support with a smaller lattice constant [15]. Alternatively, an effective compressive strain can also be produced by embedding the metal atom in a surface alloy layer with a fixed overall lattice, where the other metal species has a larger atom size. These geometric effects

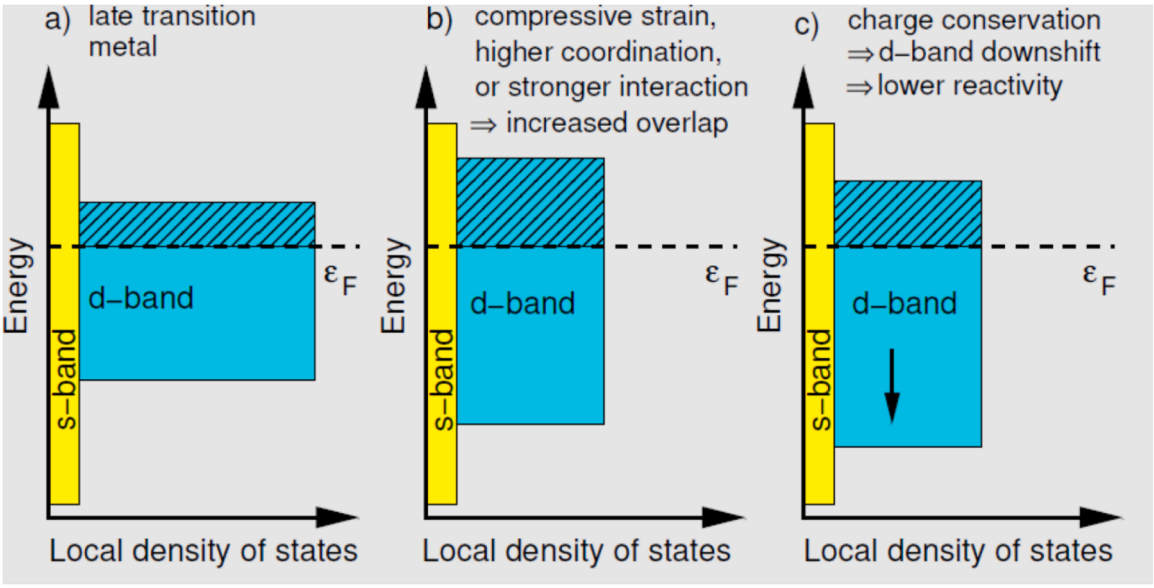

Fig. 2. Illustration of the effect of compressive strain or increased coordination on the width and position of the d-band of a late transition metal: (a) more than half-filled d-band; (b) increased width of the d-band due to a compressive strain or higher coordination; (c) down-shift of the d-band relative to (b) because of charge conservation (hatched: density of unoccupied states).

(strain effects) lead to an increased overlap of the metal orbitals, which results in a larger local band width (see Fig. 2b), similar to the increased splitting between bonding and antibonding orbitals in molecular chemistry with increased overlap. Of course, there are also situations in which the d-band width becomes smaller, e.g., due to tensile strain or weaker interaction with neighbors. In this case, the d-band center of a late transition metal shifts upwards, leading to a stronger metal-adsorbate bond.

In a simple tight-binding picture, the band width is furthermore linearly related to the coordination of the atom [112]. Hence, a higher coordination also increases the band width, which results in a weaker bond between this surface atom and an adsorbed species. Correspondingly, lower coordination as experienced for step and kink atoms (undercoordinated sites) leads to stronger adsorption bonds. This effect, which corresponds closely to the principle of constant bond order (see discussion below), was demonstrated both experimentally ad theoretically. Experimentally, such a trend was reported, e.g., for CO adsorption on stepped Pt(111) surfaces [113–116] and for CO and oxygen adsorption on a curved Pt surface, where the adsorption strength was found to increase in the order $E_{ad,terrace\ site} < E_{ad,step\ site} < E_{ad,kink\ site}$ [117]. Theoretically, Hammer et al. demonstrated this trend for CO adsorption on terrace, step and kink sites of different Pt surfaces based on the d-band model [118].

Apart from these geometric effects, there is also an electronic effect, the so-called ligand effect [9,11–14], which is caused by the electronic interactions between the different components of a bimetallic system. A metal atom A neighboring to a metal atom B with a higher adsorption strength than A will experience a stronger interaction with this hetero atom B than in A-A bonds. This will then also lead to a larger local band width on both surface atoms A and B. As discussed above, increasing the d-band width will lead to a down-shift of the d-band and the d-band center, which is associated with a lower local reactivity of the surface atom A, i.e., the interaction with adsorbates becomes weaker. Also in this case an opposite shift / no shift are expected for early transition metals (d-band less than half filled) or for metals with a filled d-band.

These considerations with respect to the geometric and electonic effects can qualitatively also be described in a simple bond order concept [18,119]. The situation depicted in Fig. 2b corresponds to an increase of the bond order of the considered surface metal atom, as either the number of the chemical bonds with the neighboring atoms or their strength is increased. The higher the bond order of an atom is, the less prone the atom is to make additional or stronger bonds to other species such as adsorbing atoms or molecules. Thus, a higher bond order of the respective surface atom leads to a lower bond strength to adsorbed species, which in the d-band model is reflected by a down-shift of the d-band center.

Finally, we would like to get back to the case of early transition metals with a less than half-filled d-band. As already mentioned, in this case the charge conservation argument would lead to an opposite trend in the d-band shift as depicted in Fig. 2. Increasing the coordination of the metal surface atoms or applying compressive strain would lead to an up-shift of the d-band and thus to a strengthening of an adsorption bond, opposite to the trend in late transition metals. This trend has indeed been observed in some early transition metals such as Sc, V and Ti, and has been demonstrated for H adsorption energies [120]. Hence, while the d-band model still results in a correct prediction of the trend in adsorption energies, the correlation with the bond-order concept does not work any more, as the latter would predict a weakening of the metal-adsorbate bond for higher coordination of the metals surface atoms. Nevertheless, considering that most metal or bimetal catalysts involve late d-band metals, the description of trends in adsorption energy in terms of the constant bond order principle is of great practical use.

2.4. Stability of bimetallic surfaces

The thermodynamic stability of bimetallic surfaces is generally related to their surface energies and their formation energy. Although the Gibbs free energy would be more relevant, it is mostly not used because of the unknown contribution from configurational entropies. Their calculation would require a precise knowledge of the distribution of the respective atoms in the bulk and in the surface region, which is mostly not available. The surface energy, or more correctly, the specific surface energy of a solid, E_S, is classically defined as the energy required to reversibly increase the surface area A of a given solid, while keeping the mass constant

$$E_s = \frac{\delta E}{\delta A} \tag{1}$$

Following this definition, the surface energy determines, e.g., the energetically most preferential shape of a crystal, which can be determined via the Wulff construction [121], or the thermodynamic growth modes during epitaxial growth in an epitaxial system [42,43]. Correspondingly, the formation energy will determine the stability of a given mixed phase as compared to that of a phase separated system. Kinetically, the stability against faceting or against alloy formation or surface segregation will be affected by these quantities.

Unfortunately, the quantitative determination of surface energies is not only experimentally, but also theoretically challenging, at least in an atomistic picture, e.g., by using periodic density functional theory (DFT) based calculations [122]. Surface energies of solids have commonly been calculated as the cleavage energy of a bulk crystal along a given plane, by subtracting the bulk energy of the solid from the energy of a limited slab with a defined surface area A and the same number of atoms per unit cell, E_{slab}, via

$$E_S = {}^1/_{2A}(E_{slab} - E_{bulk}) \tag{2}$$

The calculation of surface energies requires the use of thick slab models as both sides of the slab need to be relaxed, whereas asymmetric slab models (see Fig. 3a) yield an average surface energy of a relaxed and a frozen surface structure. However, there is also a procedure how from such an asymmetric calculation the surface energy of the relaxed surface can be derived [60,61,123–128]. In the case of compounds or bi- or multimetallic systems, the situation is even more complex, as illustrated in Fig. 3b for a system consisting of a support covered by a film of one or a few layers thickness. In this case, the surface energies at the top surface and at the bottom surface are likely to differ significantly, and calculations according to Eq. (2) would yield an average value of the two surfaces. Furthermore, since the surface energy of a given surface will depend on the nature of the bonds that have to be broken, it will depend on the nature and structure of the layers on the other side of the intended cleavage planes. This had been discussed in detail in Ref. [122]. As described there, the initial crystal should most simply be symmetric with respect to the cleavage plane, both structurally and with respect to the chemical composition of the respective layers on both sides of the cleavage plane. Such kinds of model systems, which would resemble also the situation in an elemental system, are, however, more complex than the model systems used in standard DFT calculations, and have to be constructed for the given system. As an example, in such an approach the

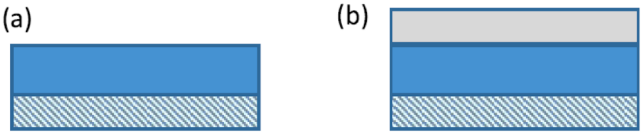

Fig. 3. Asymmetric slab models for monometallic (a) and bimetallic (b) unit cells and slabs, illustrating their asymmetric nature (blue hatched: frozen support bottom layers, blue: relaxed support layers at/close to the surface, gray: deposit). Reprinted from Sakong et al. [122], published under a CC BY license.

surface energy of the Ag-terminated surface of a pseudomorphic monolayer Ag film on a bulk support Pt(111), which is modelled by 5 Pt layers ($Ag_{1L}/Pt_{5\ L}$), would be calculated as the cleavage energy of a mirror-symmetric slab with 10 Pt layers in the center, followed by 1 pseudomorphic layer of Ag in each direction, where the cleavage plane is above (below) the Ag monolayer (see Fig. 4). In a similar way, the surface energy of the (bottom) surface of the n-layer Pt(111) support (Pt-terminated slab) can be calculated, which for a reasonable thickness of the support model should quickly approach the surface energy of pure Pt(111) (for details see [122]).

The use of appropriate model systems is particularly important, e.g., in cases where calculated surface energies and interface energies are used for predicting thermodynamic growth modes in epitaxial systems.

The second parameter important for the stability of bimetallic surfaces is the formation energy E_f (or H_f, when referring to the formation enthalpy). Following the classic definition in thermodynamics, it describes the energy gained or required for creating a system from the atomic species in a bulk reservoir, using the bulk energies E_i of the individual components i via

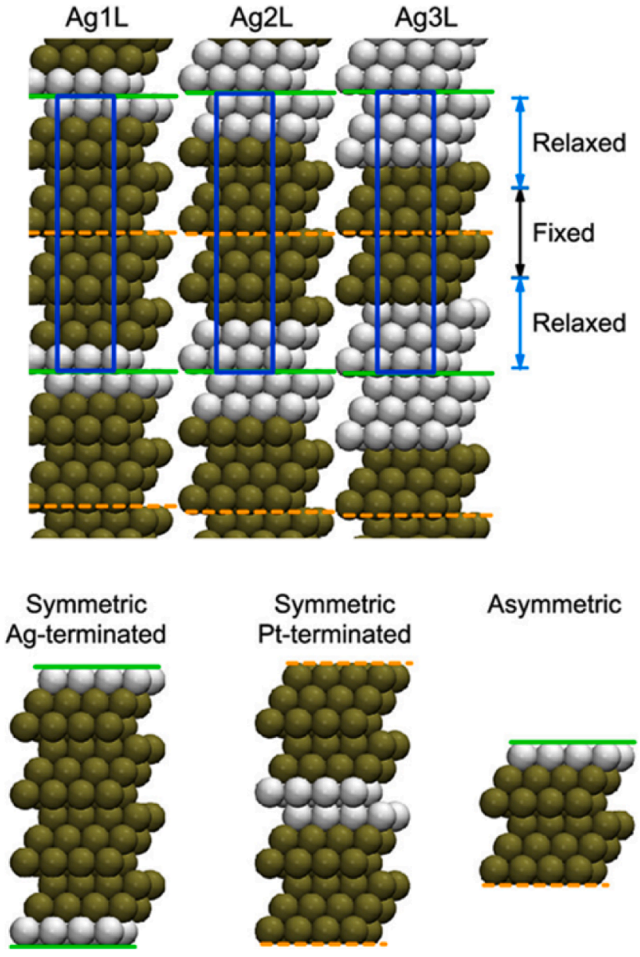

Fig. 4. Models of the symmetric 12-layer bulk supercells (top row) and of the similar size Ag-terminated and Pt-terminated symmetric slabs (here: for Ag1 L, bottom row) used in reference [122] for calculation of the surface energies etc. of different Ag/Pt(111) systems (light gray: Ag, olive: Pt) for systems with Ag films of 1, 2 or 3 layers thickness. The blue box shows the unit cell of the bulk. Cleaving along the planes indicated by the green solid and orange dashed lines in the bulk presentations generates the symmetric Ag-terminated slab and Pt-terminated slabs, respectively, from the periodic bulk, which are shown in the bottom row. In addition, we also show the asymmetric 6-layer slab (bottom row), which is normally used for such calculations. Adapted from Sakong et al. [122], published under a CC BY license.

$$E_f = E_{sys} - \sum_i n_i \cdot E_i \tag{3}$$

where E_{sys} denotes the energy of the system and n_i the number of atoms of type i in the system. Note that the formation energy depends on the size of the system and is typically normalized by the number of atoms or by the size of the surface area A of the (bulk) unit cell. Considering that the unit cell includes surfaces on the top and on the bottom side, the formation energy is generally normalized by $2A$ rather than by A, leading to

$$E_f = \frac{1}{2A}\left(E_{sys} - \sum_i n_i \cdot E_i\right) \tag{4}$$

Furthermore, one may distinguish between bulk and slab formation energies, $E_{f,bulk\ and}\ E_{f,slab}$ respectively, depending on whether it this calculated for a unit cell in the bulk or for a slab, where the latter contains also contributions from the surfaces [122].

Barabash et al. [129] had proposed to determine the (slab) formation energy $E_{f,slab}$ of a bimetallic surface region using the pure support as reference. It describes the change in slab energy from the initial monometallic slab ($E_{slab,in}$) upon exchange of n_i atoms of species i to/from a reservoir of that respective species to the final bi- or multicomponent slab, and can be calculated via eq. (5)

$$E_{f,slab} = \frac{1}{2A}\left(E_{slab,fin} - E_{slab,in} - \sum_i n_i \cdot E_i\right) \tag{5}$$

In that case, the formation energy of a B_{2L}/A_{nL} model system as described above would be calculated as

$$E_{f,slab,\ B_2/A_n} = \frac{1}{2A}\left(E_{slab,\ B_2/A_n} - E_{slab,A_n} - n_i \cdot (E_B - E_A)\right), \tag{6}$$

where E_A and E_B represent the bulk energies of elemental A and B, respectively, and n_i the number of exchanged atoms A. It is important to realize that the resulting formation energy is specific for a given reference system, in this case the support A (see [129] and [122] for details).

This brief summary indicates already that great care has to be taken when using calculated surface energies and formation energies of bimetallic surfaces in the discussion of surface stabilities etc., as the numbers will depend sensitively on the approach used in these calculations.

3. Chemistry of bimetallic surfaces

3.1. Adsorption properties

The adsorption properties of single-crystalline bimetallic surfaces differ from those of monometallic / elementary surfaces by the existence of a large number of different adsorption sites. While on smooth, ideal elementary surfaces the sites differ only by their coordination, i. e., by the number of surface atoms contributing to the adsorption site, such as adsorption on on-top sites (1 atom), on bridge sites (2 atoms) or on threefold sites (3 atoms), (smooth) bimetallic surfaces offer a large variety of sites or adsorption ensembles of different composition. For AB-type mixed surfaces, they may include A, B, AA, AB, BB, A_3, A_2B etc. sites. Furthermore, also the neighbors of the respective adsorption ensemble, including both atoms directly aside and/or directly underneath the respective surface ensemble, may modify the adsorption properties of these sites by electronic interactions (ligand effects) or by imposing lattice strain (strain effects [15]). Thus, the concepts of the (geometrical) ensemble effect and the (electronic) ligand effect, which had been initially introduced in the discussion of the catalytic activity of bimetallic catalysts (see Sections 1. and 3.2 as well as references [7–13]), are equally applicable also for the description of adsorption properties. In fact, these modifications of the adsorption properties

provide the rational basis for the trends in the catalytic activity of these systems.

In the following, we will illustrate these concepts and more recent developments using structurally well-defined PtAg and PdAg surfaces as example, which have been investigated extensively both in our groups [57,58,60,61,123–128] as well as in others [62,70,72,77,95,130–132]. These surfaces include Pd(111) and Pt(111) surfaces modified by ultrathin Ag films [60,77,126] or surfaces covered by monolayer surface alloys, where a pseudomorphic PdAg or PtAg layer is supported on a Pd (111) or a Pt(111) support, respectively. Alternatively, PtAg or PdAg surfaces were prepared also by deposition of Pt or Pd on Ag(111) supports [69–74,95]. In an atomic picture, these surface alloy systems differ from the surface region of comparable bulk alloys by the homogeneous local composition and structure of the underlying second and deeper layers, which simplifies the identification and classification of different adsorption sites enormously. Nevertheless, we will compare these results also with comparable data obtained in adsorption studies performed on PdAg bulk alloys [133–135], while no such studies were found for PtAg bulk alloys. In the following, we will discuss tests of the adsorption properties of various PtAg and PdAg surfaces using CO and hydrogen as probe molecules / atoms, and compare them with structural information to identify local adsorption properties on these surfaces.

3.1.1. CO adsorption on PtAg and PdAg surfaces

For CO adsorption on the partly or fully Ag film covered Pt(111) [126] and Pd(111) [60,77] surfaces, the rather inert Ag mainly acts as blocking species, at least during CO adsorption at room temperature and higher. Upon CO adsorption at liquid N_2 temperatures, CO desorption from Ag/Pt(111) is observed in a small peak at 130 K [126] (see Fig. 5). Note that this desorption temperature is much higher than CO desorption from Ag(111) (desorption temperature around 50 K [136]). The main peak centered at about 380 K is due to desorption from Pt(111) sites. Finally, a small CO desorption peak above 500 K, which grows upon annealing to > 600 K and subsequent exposure to CO, was associated with CO strongly bound to Pt atoms (partly) surrounded by Ag

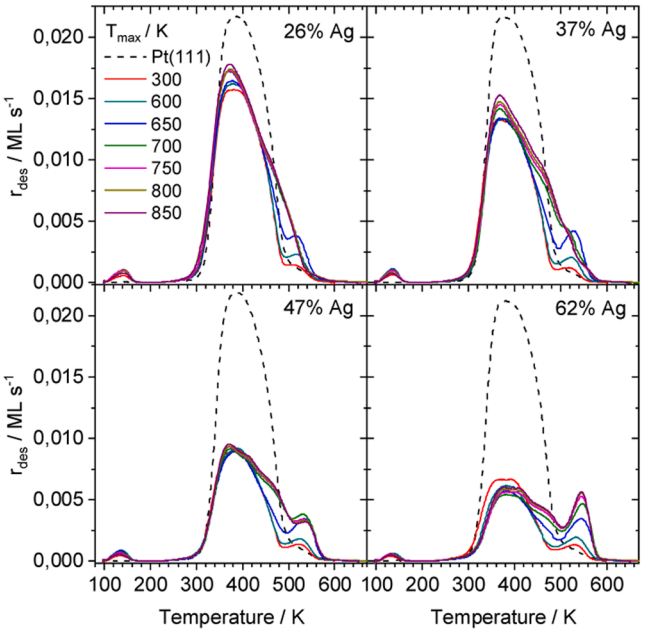

Fig. 5. CO-TPD spectra obtained after CO_{ad} saturation at 100 K of Pt(111) surfaces covered by Ag films or mixed PtAg layers with different Ag surface concentrations (see figure), following Ag deposition at room temperature (300 K) and subsequent heating to successively higher temperature, as indicated in the figure. For comparison: spectrum obtained for pure Pt(111) (dashed lines). Adapted with permission from Ref. [126], Copyright 2015 Wiley-VCH Verlag GmbH & Co. KGaA, Weinheim.

atoms [126]. A similar peak was observed also during CO desorption from a fully Ag covered surface (3 monolayers (ML)) after annealing ≥ 900 K, where Ag starts to desorb and Pt starts to segregate to the surface [126]. In combination, this indicates that neighboring Ag atoms lead to an increase in Pt-CO bond strength. These results fit well to those of an IR spectroscopy study on the adsorption of CO on similar Ag covered Pt (111) surfaces by Rodriguez et al. [77]. Those authors reported that CO adsorbed on Ag deposited at 90 K, which leads to very small Ag defect structures with a large number of undercoordinated Ag sites, desorbs at about 70 K higher temperature than from smooth Ag(111) films. Stepwise annealing a 1.3 ML Ag covered Pt(111) surface and subsequent saturation of CO led to a continuous decay of the CO-Ag/Pt(111) related IR band intensity, which was attributed to the formation of a smoother Ag film with fewer more strongly adsorbing Ag defect sites. The appearance of a new band at 2134 cm^{-1} for CO on a 500 K annealed Ag/Pt(111) surface, which was not commented upon in [77], is likely due to the formation of new Ag-Pt sites at the onset of intermixing, in agreement with comparable findings for CO adsorption on 600 K annealed Ag/Pt(111) surfaces by Diemant al. [126]. Note that these results are consistent with expectations based on the constant bond order concept (see Section 2.3), if the CO species desorbing at 130 K represents CO adsorbed on undercoordinated Ag step and kink sites, while adsorption on Ag atoms within pseudomorphic Ag islands should be weaker than on Ag(111) because of the stronger interaction between Ag surface atoms and the Pt(111) support atoms compared to Ag-Ag bonds (ligand effects) and due to the compression of the 2D Ag layer (strain effects).

For Ag/Pd(111), neither desorption at 130 K nor a distinct higher-temperature CO desorption peak (at ~550 K) were observed, indicating that similar PdAg configurations either do not exist or do not lead to a stabilization of the CO-Pd bond. The absence of CO adsorption on Ag monolayer films on Pd(111) at temperatures above 90 K, as observed in this study, suggests a weak Ag–Pd interaction, and also agrees with recent calculations indicating that the Ag valence band in 1–2 ML Ag films is only weakly perturbed by the underlying Pd support [80]. It also agrees with calculations, which show a significantly lower CO adsorption energy on monolayer Ag/Pd(111) systems than on Ag/Pt(111) [124,127].

Moving on to CO adsorption on PtAg/Pt(111) and PdAg/Pd(111) monolayer surface alloys, we can compare experimentally determined CO and H_2 adsorption properties with adsorption energies and trends in vibrational frequencies calculated for adsorption on different adsorption ensembles. As discussed already above, CO TPD spectra recorded after CO saturation of PtAg/Pt(111) surfaces with different Ag contents (see Fig. 5) at 100 K, which before CO adsorption were annealed to the temperatures indicated, showed little change upon annealing, except for the formation of the small higher-temperature peak with a maximum at about 525 K. For comparison, Schüttler et al. performed density functional theory based (DFT) calculations for CO adsorption on a number of different Pt_n ensembles, which were surrounded by Ag surface atoms and pseudomorphically grown on Pt(111) [127]. In these calculations, the authors considered CO adsorption on Pt_1 monomer sites, on Pt_2 dimer sites, and on compact Pt_3 trimer sites (Fig. 6). Adsorption on a surface with Pt_1 monomers is most stable on the on-top adsorption site, since bridge bonded adsorption on PtAg sites or on $PtAg_2$ sites is much weaker [127]. For CO adsorption on Pt_2 dimer sites, there is almost no difference between on-top adsorption on one of the two Pt surface atoms and adsorption in a bridge-bonded configuration, and the same is obtained also for adsorption on a Pt_3 trimer [127]. Furthermore, the adsorption energy is almost constant for on-top adsorption on the different ensembles, with only a very small decay in the order Pt_3 - CO < Pt_2 - CO < Pt - CO [127,128]. Also CO_{ad} coverage effects are small, with only slight losses in adsorption energy when going from 1 CO_{ad} to 2 or 3 CO_{ad} per Pt ensemble, and similar trends are observed also for CO adsorption on larger Pt_n ensembles [128]. Furthermore, different from CO adsorption on Pt(111), local coverages of 1 CO_{ad} per Pt surface atom

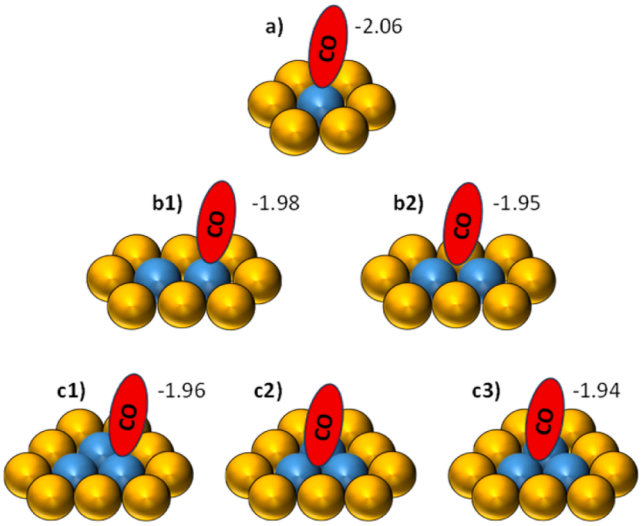

Fig. 6. Schematic ('bird eyes') representation of CO adsorption in an on-top configuration on a Pt_1 monomer (a), in an on-top and in a bridged configuration on a Pt_2 dimer (b1 and b2), and in an on-top configuration, on a bridge site and on a threefold hollow site on a Pt_3 trimer (c1, c2 and c3) in monolayer PtAg/Pt(111) surface alloys. Note that for symmetry reasons CO is expected to stand upright in configurations a), b2) and c3), while in the other cases a small tilt is likely. Adsorption energies in eV, where determined, were calculated with a PBE/PAW functional in [127].

can be reached. Apparently, repulsions between neighboring CO_{ad} molecules can be strongly reduced on these separated Pt_n ensembles by an outward tilting of the neighboring CO_{ad} molecules [128]. These calculated trends agree perfectly with the experimental observation of an essentially constant position of the CO desorption peak for different Pt_xAg_{1-x} compositions of the bimetallic surface layer [126].

Further experimental support of rather similar CO adsorption energies on the different sites comes from a high-resolution X-ray photoelectron spectroscopy (XPS) study by Bauer et al. [62], who observed the simultaneous appearance and disappearance of two C1 s peaks with different binding energies (BEs) during adsorption and desorption of CO on PtAg/Pt(111) monolayer surface alloys. Based on rather similar observations for CO adsorption on Pt(111) [137], they explained this by a simultaneous population and de-population of bridge and on-top sites during CO adsorption / desorption. The only difference between their results and the above theoretical prediction, the absence of CO_{ad} on threefold sites on Pt_3 and larger ensembles at low CO_{ad} coverages in their measurements, may be due to either the slightly lower adsorption energy on these sites (see Fig. 6) and/or small differences between the C1 s BEs of CO adsorbed on bridge or threefold sites.

In total, these data indicate that for PtAg/Pt(111) surface alloys electronic ligand effects and geometric strain effects almost compensate each other. Strengthening of the Pt-CO bond due to the weaker Pt-Ag bonds with neighboring Ag surface atoms is essentially compensated by the Pt-CO bond weakening induced by the larger size of the neighboring Ag surface atoms and the resulting compressive strain on the Pt ensemble. Similar to CO adsorption on Pt(111) [138], the energy differences between adsorption on on-top sites, bridge sites and threefold hollow sites are small.

Finally, these calculations also revealed that the simultaneous adsorption of 2 CO on a Pt_1 monomer is instable compared to 1 adsorbed CO and 1 gas phase CO [128]. This agrees with experimental findings in so far as the formation of multicarbonyl species, which is often discussed in the literature for Ru nanoparticles [139–141], has rarely been proposed for Pt nanoparticle catalysts [142,143].

Despite the very similar structural and electronic properties of the two support surfaces, the situation is very different for CO adsorption on PdAg/Pd(111) surface alloys [60,61,124]. Saturation CO-TPD spectra recorded on surface alloys prepared by deposition of 1.2 monolayers of Ag on Pd(111) and subsequent annealing to increasing temperatures show a continuous shift of the CO desorption peak up to 800 K annealing [60]. Annealing to even higher temperatures leads to the appearance of new peaks on the low-temperature and high-temperature side of the main peak, until upon annealing to 1100 K Ag is completely desorbed / dissolved in the bulk and the TPD spectrum resembles that of CO desorption from Pd(111) [60]. More information is obtained from CO TPD series recorded on PdAg/Pd(111) monolayer surface alloys with different Pd surface contents, which at the lowest Pd concentrations (2 %) show a peak at 316 K [61]. This was associated with CO desorption from Pd_1 monomers surrounded by Ag surface atoms. At higher Pd contents, between 7 % and 10 %, this peak up-shifted to 364 – 380 K, with a shoulder at about 320 K. These features, which became more pronounced for 25 % surface Pd, were attributed to desorption of two CO from Pd_2 dimers, with the first one desorbing at 320 K and the second one at 380 K (see discussion of CO coverage effects with Fig. 8). At even higher Pd surface concentration ($\geq$ 39 %), a peak at about 460 K appeared, which was related to CO desorption from threefold hollow sites on Pd_3 or larger ensembles [61]. Pronounced differences compared to the CO adsorption behavior on PtAg/Pt(111) surface alloys were obtained also in DFT calculations performed for CO adsorption on PdAg/Pd(111) surface alloys [124]. The resulting CO adsorption energies, obtained for the same adsorption ensembles and sites as in Fig. 6 for PtAg/Pt(111), are presented in Fig. 7. These calculations also show a strong preference for adsorption on threefold hollow sites, similar to CO adsorption on Pd(111) [144,145], with the CO adsorption energy increasing in the order $E_{ad,on\text{-}top} < E_{ad,bridge} < E_{ad,hollow\ site}$. On the other hand, there is very little change in the (calculated) adsorption energy on the same site when going to larger ensembles, e.g., for on-top adsorption when going from Pd_1 via Pd_2 to Pd_3, indicating that similar to CO adsorption on PtAg/Pt(111) lateral ligand and strain effects largely compensate each other. This conclusion is supported also by the calculated result that Pd_3 and Pd_4 (not shown) exhibit similar CO adsorption energies on the threefold adsorption sites. This suggests that adsorption on Pd_3 sites largely determines the highest adsorption energy and that

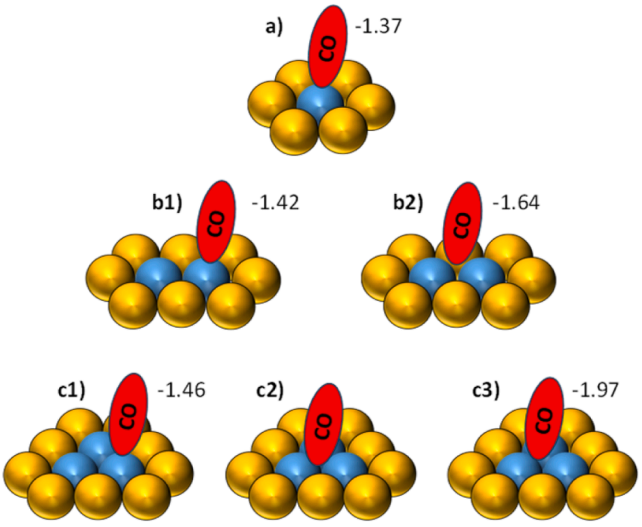

Fig. 7. Schematic ('bird eyes') representation of CO adsorption in an on-top configuration on a Pd_1 monomer (a), in an on-top and in a bridged configuration on a Pd_2 dimer (b1 and b2) and in an on-top configuration, on a bridge site and on a threefold hollow site on a Pd_3 trimer (c1, c2 and c3) in monolayer PdAg/Pd(111) surface alloys. Note that for symmetry reasons CO is expected to stand upright in configurations a), b2) and c3), while in the other cases a small tilt is likely. Adsorption energies in eV, where determined, were calculated with a PBE/PAW functional in [124].

the effect of additional surrounding Pd ligands is small. In this sense, experimental results (TPD peaks, infrared bands) attributed to Pd_3 ensembles may originate not only from Pd_3, but also from larger ensembles [124]. Finally we would like to add that these desorption temperatures are very close to those reported for CO desorption from Pd_1 monomers (300 K) and Pd_2 dimers (360 K) in a PdAu surface alloy on Pd(111), indicating rather similar ligand and strain effects in both cases [146].

Furthermore, these calculations also revealed significant vertical ligand effects on the CO adsorption behavior, which are reflected by a lower CO adsorption energy on Pd_n surface ensembles that are separated from the bulk by a pseudomophic Ag layer [124]. This agrees well with the down-shift of the local d-band center calculated for these sites [124] and with the experimental observations of a reduced CO adsorption energy on on-top sites of Pd monomers surrounded by Ag atoms also in the second layer [61]. The trend seems to differ from expectations based on a simple bond order picture, since one would expect a stronger Pd-CO binding on such sites, due to the weaker Pd bonding to the underlying Ag atoms instead of Pd atoms. Looking more closely, however, we have to consider that also the interaction between Ag atoms in the surface layer and those in the Ag second layer is weaker than the interaction with a Pd second layer. This results in a stronger interaction between Pd surface atoms and neighboring Ag surface atoms (Ag ligands), which leads to a weaker Pd-CO bond. Apparently, this effect overcompensates the Pd-CO bond strengthening expected from the vertical ligand effect (interaction of surface Pd with Ag in the second layer), which would lead to a stronger Pd-CO bond. This case demonstrates nicely that the prediction of trends in adsorption energies can be difficult in complex situations like the above example, where several counteracting effects have to be considered. Nevertheless, in most situation it allows a simple estimate of trends in adsorption energies.

Next, we will compare the CO_{ad} coverage effects for PdAg/Pd(111) with those obtained for PtAg/Pt(111) (see above). Different from the latter systems and from CO adsorption on Pt(111) [126,147,148], CO adsorption on PdAg/Pd(111) shows considerable coverage effects, when comparing, e,.g., adsorption of a single CO on a Pd_2 with adsorption of two CO on that ensemble [124]. This is also indicated by the appearance of additional lower temperature peaks in the TPD spectra [61]. A more detailed inspection revealed, however, that the decrease in effective adsorption energy is mainly due to changes in the adsorption site rather than directly caused by CO_{ad} – CO_{ad} repulsions. This is illustrated in Fig. 8. While compared to adsorption on the most stable sites of Pd_2 dimers or Pd_3 trimers the mean adsorption energy of two or three on-top adsorbed CO is drastically reduced, by 0.33 eV per CO_{ad} (Pd_2 dimer) or even by 0.68 eV (Pd_3 trimer), the actual effect of the (repulsive) CO_{ad}–CO_{ad} interaction is much less. This is illustrated by using adsorption of a single CO_{ad} on an on-top site of the respective ensemble as reference. In this case, the binding strength of the second CO_{ad} decreases much less, from −1.42 eV to -1.20 eV, due to the mutual repulsion of the CO

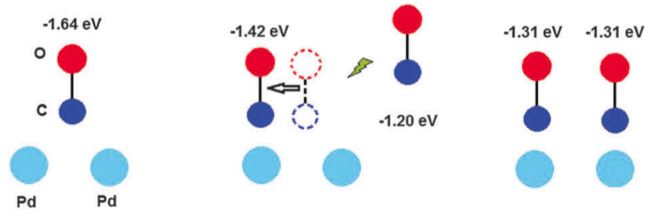

Fig. 8. Simplified illustration of CO adsorption on a Pd_2 ensemble at higher coverages. Left: preferred adsorption of one CO molecule at the bridge site of Pd_2. Center: energetics relevant to the adsorption of an additional CO molecule on the Pd_2 dimer. Repulsion from neighboring CO molecules shifts the first absorbed CO molecule away to an on-top site and reduces its adsorption energy. A second CO molecule will be adsorbed on the other on-top site. Right: final state, showing simultaneous adsorption on the two on-top sites with their mean adsorption energy (Pd: cyan, C: blue, O: red). Reprinted from Mancera et al. [124], with permission of the Owners Societies.

molecules at the adjacent top sites. The remaining 0.22 eV is needed to displace the initial CO_{ad} from the most stable bridge site to an on-top site (Fig. 8, middle).

As indicated before, we will also briefly compare CO adsorption on the surface alloys with that on $Pd_{67}Ag_{33}(111)$ bulk alloys [133–135]. This surface differs from the PdAg/Pd(111) surface alloys by its slightly larger lattice constant and by the presence of Ag atoms also in deeper layers, leading to a modification in strain effects and in vertical ligand effects. TPD spectra recorded on CO covered $Pd_{67}Ag_{33}(111)$ (CO adsorption at about 270 K) revealed a single peak only, with a maximum at about 370 K [133,134]. This closely resembles the observations obtained for CO desorption from PdAg/Pd(111) surface alloys with surface Pd contents between 7 % and 10 %, which was attributed to desorption from Pd_2 ensembles [61]. The Pd content of the $Pd_{67}Ag_{33}(111)$ surface in that study was estimated to be around 10 % [133], which is less than half of the Pd content in the PdAg surface layer in the PdAg/Pd(111) sample shown in Fig. 1e. In a later atomic resolution STM study of a similar sample, Wouda et al. determined a Pd surface content of about 5 %. In that case they obtained dominant Pd_1 monomers and Pd_2 dimers on the $Pd_{67}Ag_{33}(111)$ alloy surface [149]. Considering the different procedures for surface preparation, these results agree very well and fit perfectly to the results obtained for CO adsorption on the PdAg/Pd(111) surface alloys. Hence, CO adsorption on this bulk alloy surface seems to closely follow the trend derived for the PdAg/Pd(111) surface alloys, and the combined differences in the ligand and strain effects are small.

As a last point, we briefly compare with CO adsorption on PdAg/Ag (111) [95] or PtAg/Ag(111) [70,150] surface alloys, which were prepared by deposition of Pd or Pt on a Ag(111) support [69–74,95]. Also these samples differ from the Pd(111) or Pt(111) supported surface alloys by the different lattice constant, which for pseudomorphic films results in very different strain effects, by the different vertical ligand effects (Pd-Ag instead of Pd-Pd interaction), and in particular by their much higher tendency for intermixing.

For CO adsorption on PdAg/Ag(111) surface alloys with very low Pd contents, prepared by Pd deposition at room temperature, Muir et al. reported a CO desorption peak at 279 K, which they attributed to CO desorption from Pd_1 monomers [95]. At a higher Pd coverage, a second desorption peak appeared at 370 - 390 K, assigned to CO desorption from Pd_2 bridge sites. These desorption temperatures are rather close to the peaks at 316 K and 364 – 380 K reported for CO desorption from on top adsorption on Pd_1 monomers and bridge bonded CO on Pd_2 dimers in PdAg/Pd(111) surface alloys [61]. Hence, the additional strain effects and vertical ligand effects introduced when changing from Pd_1 monomers and Pd_2 dimers in a PdAg surface layer on Pd(111) to Ag(111) result only in a rather small increase in CO adsorption energy for adsorption on a Pd_2 site, while for adsorption on Pd_1 monomers it is more pronounced. Calculations for CO adsorption on PdAg/Ag/Pd(111) had shown that the presence of one or two Ag underlayers on Pd(111) underneath the PdAg surface layer leads to a decrease of the CO adsorption energy [124], while the larger lattice constant of Ag(111) should lead to an increase. Hence, these effects will partly compensate each other, which explains at least qualitatively the little difference in CO binding energy on Pd_1 monomers and Pd_2 dimers between these two systems.

For CO adsorption on PtAg/Ag(111) surface alloys with low Pt contents, prepared by Pt deposition at 380 K, Patel et al. reported a CO desorption peak at 380 K, which they attributed to CO adsorption on Pt_1 monomers [70]. At higher Pt surface contents (> 20 %), a second peak at 477 K appeared, which the authors assigned to desorption from Pt ensembles. These desorption temperatures are significantly higher than those obtained for desorption from PdAg/Ag(111) surface alloys [95], which we mainly relate to the much more pronounced ensemble effect for CO adsorption on Pd_n ensembles than on Pt_n ensembles. While CO adsorption on threefold sites on Pd_3 or larger ensembles is significantly stronger than on-top adsorption on Pd_1 monomers, the differences are much smaller for adsorption on Pt_n ensembles, with only a small

preference for CO adsorption on-top sites (Fig. 6). All in all, the differences in CO adsorption on these two types of surface alloys, PdAg/Ag(111) and PtAg/Ag(111), can be explained in a consistent picture, and the same is true also for the differences in CO adsorption when changing the support from Pd(111) or Pt(111) to Ag(111).

3.1.2. Hydrogen adsorption on PdAg surfaces

Finally, we want to illustrate the role of ensemble effects, using the adsorption of hydrogen on PdAg/Pd(111) monolayer surface alloys as example. This differs from the situation experienced for CO adsorption in two aspects. First, stable adsorption on metals at room temperature is only possible for atomically adsorbed H_{ad} (dissociative adsorption), which means that 2 H_{ad} atoms have to be accommodated per adsorbing H_2 molecule. Second, adsorption of H_{ad} on a Ag monolayer on Pd()111) is instable [125]. If diffusion of individual H_{ad} from one Pt_n ensemble to another one is inhibited, both H_{ad} species resulting from an impinging H_2 molecule have to be accommodated on the same Pt_n ensemble for a successful adsorption process.

To test this idea, we compared calculated binding energies for 2 H_{ad} on different Pt_n ensembles on these PtAg surface alloys and compared them with experimental temperature programmed desorption (TPD) spectra [125]. As evident from Fig. 9, desorption from surfaces with Ag surface contents of up to 50 % shows 3 distinct desorption peaks g_1, g_2 and b. Based on DFT calculations, these desorption peaks can be attributed to associative desorption of 2 H_{ad} from Pt_2 ensembles (γ_1-peak), Pt_3 or Pt_4 ensembles (γ_2-peak) and Pt_5 or larger ensembles (β-peak) [125]. As expected, for larger Pt surface concentrations, where isolated Pt_1 – Pt_4 ensembles become less frequent, the low-temperature peaks rapidly decay in intensity.

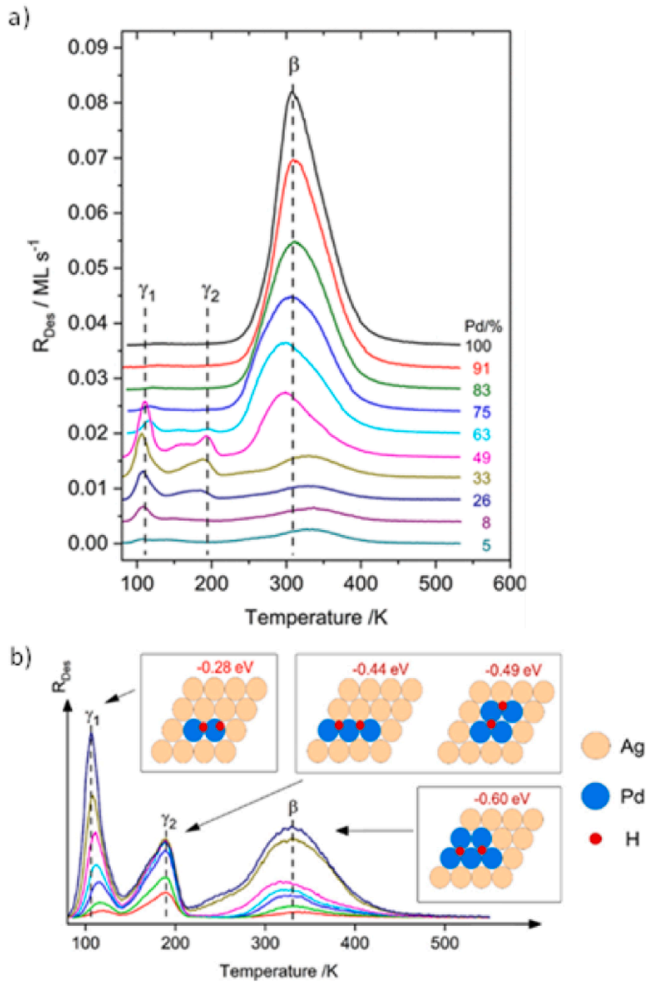

Fig. 9. (a) Set of H_2-TPD saturation spectra recorded after H_2 exposure to a PdAg/Pd(111) surface alloys with different Ag surface contents (see figure) at 100 K. (b) H_2 adsorption energies (in eV per H_{ad}) calculated for adsorption on the different Pd_n ensembles on a PdAg/Pd(111) monolayer surface shown in the figure. Adapted with permission from Mancera et al. [125], Copyright 2022 American Chemical Society.

Interestingly, these three peaks are populated simultaneously during increasing hydrogen exposure (Fig. 10), which is in contrast to the normal behavior where the most stable sites, equivalent with the highest temperature peak, is filled first. This can be simply explained in a picture where surface diffusion of H_{ad} species from one Pt_n ensemble to another one is inhibited. Thus, the different Pt_n ensembles are populated simultaneously, e.g., by dissociative adsorption of surface diffusing $H_{2,ad}$ precursor species. This perfectly confirms our above assumption that always pairs of H_{ad} have to be accommodated per adsorption of H_2. A similar behavior was obtained also for H_2 adsorption on PdAu/Pd(111) surface alloys [151], further confirming these mechanistic ideas. Finally, it should be noted that, according to the Sabatier principle (see Section 3.2), the existence of three different H adsorption sites with very different binding energies on these surfaces offers a variety of different active sites, e.g., in hydrogenation reactions.

In total, by combining structural, spectroscopic and theoretical data, these and similar type other adsorption studies have provided detailed information on the atomic-scale adsorption behavior of (locally) inhomogeneous bimetallic surfaces. This allows also to quantitatively evaluate the impact of structural and electronic effects on the adsorption behavior. Admittedly, the distinction between adsorption on different sites is more complex on surfaces where the differences in binding strength between different adsorption ensembles are less pronounced than in the examples discussed here, but it should nevertheless be possible also in such cases to identify trends.

3.2. Catalytic surface reactions

The mechanism of bimolecular catalytic surface reactions is classically described by either the Eley-Rideal (ER) mechanism [152,153], the Langmuir-Hinshelwood (LH) mechanism [152], or the Mars-van Krevelen (MvK) mechanism [154] (for an excellent review see ref. [155]). In the first case, a molecule coming from the gas phase collides and interacts with an adsorbed species, and the resulting reaction product desorbs. Alternatively, the second reactant may also be present as physisorbed species in the second layer, which is essentially identical to

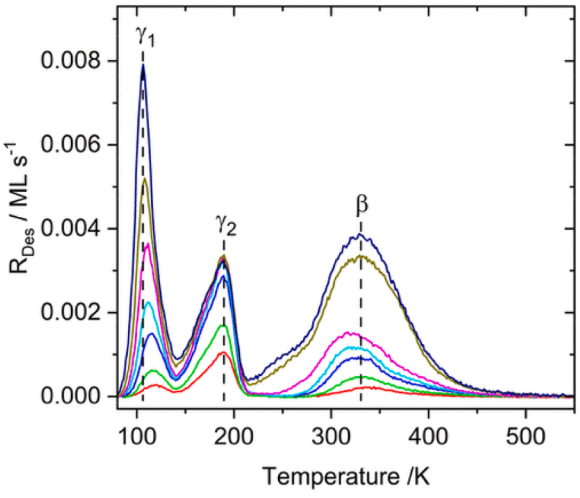

Fig. 10. D_2-TPD spectra recorded of a $Pd_{33}Ag_{67}$/Pd(111) surface alloy after increasing D_2 exposures (from bottom to top: 0.1, 0.2, 0.4, 0.6, 1, 20, and 60 × 10^{-6} mbar s). Reprinted with permission from Mancera et al. [125], Copyright 2022 American Chemical Society.

the situation in outer-sphere reactions in electrocatalysis [155]. This mechanism allows a reaction to proceed also on a surface that is completely covered by the chemisorbed species. In the LH mechanism, both species participating in the reaction are adsorbed, which means that there is an optimum adlayer composition, where the two reaction partners are adsorbed in a 1:1 ratio. Furthermore, the adsorbed species should be intermixed rather than phase separated. Complete occupation of the surface by one of the partners would result in surface blocking, and thus would stop the reaction. Thus, there is a maximum in the reaction rate, which does not exist in the ER mechanism. In the MvK mechanism, the adsorbed reactant reacts with a surface atom of the solid, mostly with oxygen in oxides, and the resulting surface oxygen vacancy is filled by oxygen from the bulk reservoir. This reservoir is replenished in an independent process by reaction of a surface oxygen vacancy with O_2, and subsequent diffusion of a surface oxygen into the bulk reservoir.

In many surface reactions, different, competing reaction pathways are possible, and the dominant pathway will depend on the catalyst material and on the reaction conditions. As an example, it is widely agreed that CO oxidation on noble metal surfaces / catalysts will follow a LH mechanism [156], while on oxide supported Au nanoparticle catalysts, where O_2 dissociation on the Au nanoparticles is strongly hindered, a Au-assisted MvK mechanism had been proposed [157,158].

The activity of (monometallic) catalysts in a given catalytic reaction was attributed to electronic properties such as the electron concentration [1], the electronic work function or the electronic density of states at the Fermi level and the gradient of the latter [2] (see also Section 2.3). In a different picture, the geometry of the adsorption site ('geometric factor') was considered as decisive parameter, in particular for reactions involving larger organic molecules [159].

These concepts and mechanistic ideas were also applied to reactions on bimetallic catalysts. For a series of binary solid solutions containing one group 8 element (Ni, Pd or Pt) together with one of group I (Cu, Ag or Au) and the binary alloys of iron, cobalt and nickel, the efficacy in multiple bond saturation or in dehydrogenation was suggested to largely depend on the number and the characteristics of the holes in the d-bands of the alloys [2,22,98]. Later, electronic effects were discussed in a more local picture and the (enhanced) reactivity of bimetallic catalysts was associated with modifications of the electronic properties of a surface atom, which may represent the active site, due to interaction with different neighboring surface and subsurface atoms [12,13]. In analogy to similar effects in coordination chemistry and homogeneous catalysis, where the state and catalytic behavior of the metal center are strongly influenced by its ligands, these effects were termed as electronic ligand effects. These as well as strain effects, which reflect the effect of lattice distortions as compared to the natural lattice of the respective surface species on the electronic structure [15], can lead to changes in the adsorption energy (see Section 3.1) and thus to significant modifications in the reaction kinetics [16,17]. Also for bimetallic catalysts, geometric effects were considered as an alternative important parameter and introduced as geometric ensemble effect, which describes the influence of the size/configuration of the active surface ensembles on the catalytic activity via their concentration [7,10].

Later, Watanabe and Motoo introduced the so-called bifunctional mechanism, where on a bimetallic surface one reactant adsorbs on the one type of surface atoms and the other one on the other type of surface atoms. Specifically, for the electrocatalytic CO oxidation on PtRu alloy surfaces they proposed that the interaction of H_2O with the surface leads to the formation of adsorbed OH on the Ru atoms, while CO is adsorbed on the Pt surface atoms [160,161]. At that point, electronic modifications of the respective surface atoms were not considered. While because of the high oxophilicity of Ru this mechanism was intuitively convincing, later experimental and theoretic studies revealed that not only OH, but also CO is more strongly adsorbed on Ru surface atoms than on Pt atoms [162]. The high catalytic activity of these surfaces, which was observed experimentally, could be explained in a picture where due to the high coverages of OH_{ad} and CO_{ad} the preferential adsorption of OH on Ru surface atoms would force CO on the Pt surface sites [163]. Essentially, the bifunctional mechanism can be considered as a LH mechanism with two or more different surface sites.

The connection between physical/chemical properties and catalytic activity of a catalyst was reported already at the beginning of the last century by Sabatier [164–166], who concluded that the activity of a catalyst is given by the binding energy of the adsorbed species, and that there is an optimum in binding energy for the most active catalyst. This results in lower activities for lower or higher binding energies, the so-called Volcano plots. An early example for such kind of correlation was given by Trasatti [101] for the electrocatalytic hydrogen evolution reaction, where a plot of exchange current densities on a large number of metal electrodes versus the metal-H bond strength resulted in an essentially perfect volcano. Similar correlations were later reported also between d-band occupancy and ammonia synthesis activity [100] or the activity in the hydrogenolysis of C-X bonds (X=C, N, Cl) [167].

Before moving on to bimetallic surfaces we would like to comment on the fact that the Sabatier principle seems to work well, although it does not specify the type of bond which should neither be too strong nor too weak. It could be the strength of a reactant-metal bond or of an intermediate or of a product to the respective metal. Furthermore, it is based on thermodynamic properties, while kinetic rates are controlled by the activation energy. The solution for this apparent discrepancy is provided by two general principles, namely the so-called scaling relation in catalysis and the Brønsted-Evans-Polanyi (BEP) relation [75,168]. The scaling relation says that the adsorption energies of different species on a given surface are correlated to each other, so that when changing to a different surface the change in binding energy of a certain adsorbed species A is related via a constant factor to that of another adsorbate B. The BEP relation correlates the kinetic barrier, i.e., the energy required to reach the transition state to the energy of the initial state (reactant) and/or the final state (product). In a simple picture, a stabilization of the initial state upon changing the catalyst will result in a higher activation energy, which assumes that the transition state is affected less by this change. Correspondingly, a weaker bonding of the initial state or a stronger bonding of the final state would result in a smaller activation barrier.

For bimetallic surfaces, the simplest picture would expect a specific rate for each type of active site or better active ensemble, which is determined by the respective bond strength on this site. In this case, the total reaction rate R would be obtained by summation over the products of the number of the respective active site n_i times the rate r_i on this site, which is given by the relevant binding energy on this site

$$R = \sum_i n_i r_i \tag{7}$$

Such kind of approach was indeed described in a number of studies on the electrocatalytic oxygen reduction reaction (ORR) on different, structurally well-defined monolayer surface alloys [169–171], among them also Pt_xAg_{1-x}/Pt(111) surface alloys [171]. Using calculated O-metal bond energy on the different A_3, A_2B, AB_2 and B_3 sites as parameter - in this case threefold adsorption sites were assumed as active sites - and the abundance of the different types of threefold sites on the hexagonal surfaces as determined by statistical evaluation of atomic resolution STM images with chemical contrast [55–57], the authors could calculate relative reaction rates (exchange current densities), relative to the maximum reaction rate, for different surface compositions. The calculated volcano plot and the exchange currents calculated for the different A_xB_{3-x} ensembles (triangles) as well as the measured kinetic currents (squares) and those calculated according to Eq. (3) (circles) are presented in Fig. 11. Note that the oxygen binding energies E_O are given relative to that for Pt(111), with increasingly positive numbers indicating weaker O_{ad} bonding. For inhomogeneous surfaces, the mean O_{ad} binding energies were calculated as the mean value of the weighted binding energies on the different trimer

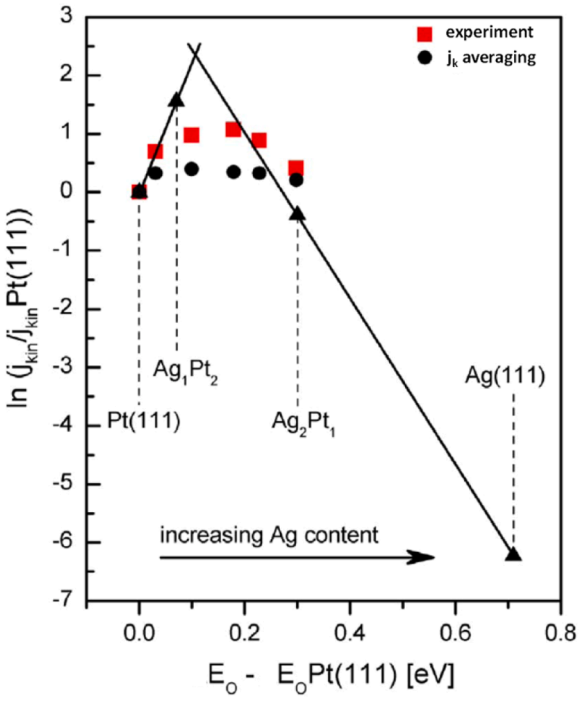

Fig. 11. Volcano plot of the relative ORR activities, both modelled and experimental, of Pt (111), of hypothetical model surfaces consisting of Ag_xPt_{3-x} trimer ensembles on a Pt(111) support (triangles) and of Ag_xPt_{1-x}/Pt(111) surface alloys of different compositions with x = 0.07, 0.19, 0.31, 0,41, 0.50 from left to right (black circles, experimental: red squares). Reprinted from Beckord et al. [171], with permission from Elsevier.

ensembles, using the trimer ensemble distribution as determined by STM. Obviously, the measured rates (squares) closely follow the calculated ones (circles). Furthermore, it is clear that the enhanced activity of the surface alloys compared to Pt(111) results from the high activity of the Ag_1Pt_2 trimer ensembles. For these sites, which except perhaps for the Ag_7Pt_{93}/Pt(111) surface alloy dominate the reaction, OH_{ad} removal represents the rate determining step, as they are still on the left slope of the volcano [171,172]. In contrast, for the Ag_2Pt_1 trimer ensemble, which is on the right hand slope of the volcano, OOH_{ad} formation would be rate limiting. Because of their much lower activity, however, the latter sites contribute little to the overall activity of the surface alloys investigated. This would be in contrast to the current mechanistic understanding that for Pt(111) OOH_{ad} formation should be rate limiting [173,174]. This and possible explanations for this discrepancy are discussed in Ref. [171]. Finally, the fact that the data calculated for the exchange current densities on the surface alloys are not exactly positioned on the Volcano can be understood from the fact that the rates are calculated as a sum of the weighted individual rates on the different ensembles rather than by averaging of the O binding energy and subsequent calculation of a rate using the mean O-binding energy.

Although this model could explain the higher ORR activity of several of the PtAg/Pt(111) surface alloys in a very satisfactory way, a later study revealed that this approach was too simple [93]. This study considered effects introduced by the surface composition on a larger scale, using a phase-separation model that allows the authors to describe the two-dimensional distribution of the Ag and Pt surface atoms and thereby the abundance of specific structural elements on a relatively large scale. Also, based on findings in recent studies [175], the authors used the *OH adsorption energies (on-top adsorption) rather than *O adsorption energies (adsorption on threefold sites) as a descriptor to estimate the catalytic activity of extended surfaces, which has considerable consequences on the geometry of suitable adsorption ensembles.

Using surface unit cells with between 100 and 900 atoms, they simulated Pt_xAg_{1-x}/Pt(111) surfaces that agreed well in the relative contributions of the Pt_xAg_{3-x} ensembles determined and used in [57, 171]. Representative configurations for a $Ag_{31}Pt_{69}$/Pt(111) surface are illustrated in Fig. 12. ORR activities were calculated by using the *OH adsorption energies on Pt or Ag surface atoms surrounded by a shell of the six nearest Pt or Ag surface atoms as a descriptor. DFT calculations performed for a large number of different heptamer configurations, including slight variations in the positions of nearest neighbors of the respective central atoms, revealed a considerable variation in OH binding energies with increasing Ag surface concentration for each of the different heptamer ensembles, and both for binding on Ag and on Pt central atoms (Fig. 13a). For Pt(Pt_6) ensembles, this amounts to about 0.1 eV (Fig. 13b). Similar variations, though less pronounced, are obtained also for the other heptamer types. Furthermore, over the entire composition range considered, up to about 60 % surface Ag, OH binding is weaker on the Pt(Pt_6) ensembles than on Pt(111), while for the other heptamer types it is stronger than on Pt(111). Hence, regardless of the configuration, the ORR activity is dominated by reaction on Pt(Pt_6) heptamers, and the enhanced activity of these binary surface alloys as compared to Pt(111) results from long-range strain effects self-induced by the surface. The Ag surface atoms in the unit cell outside the Pt(Pt_6) heptamers lead to an anisotropic compression of the Pt-Pt bonds in the Pt(Pt_6) heptamer, and thus to a strain-induced increase of the ORR activity. Additional electronic ligand effects and strain effects, in addition to the Ag-induced long-range strain effects in the Pt(Pt_6) heptamer, have little impact on the OH binding energy and thus on the ORR activity. Using the trend of the OH binding energies indicated by the black line in Fig. 13a, ORR activities can be calculated as a function of Ag surface concentrations for a wide range of concentrations. These calculations also demonstrated that the variation in ORR polarization curves obtained for Pt(Pt_6) in all different configurations was relatively small and did not affect the order of increasing activity [93].

While this result of predominant strain effects seems to be in contrast to the conclusions of the earlier study [171], the discrepancy can easily be understood by the different size of the adsorption ensembles. In [171], electronic modifications arose from changes in the composition of the direct adsorption site, the A_xB_{3-x} trimer, and strain arising for Ag outside this trimer was not included. In the study by Ozório et al. [93], the conclusion of dominant strain effects on the ORR activity refers to the ORR activity of Pt(Pt_6) heptamers and the strain induced by Ag surface atoms outside the Pt(Pt_6) ensemble, i.e., on next nearest neighbor sites relative to the central adsorbing atom or further away. Ligand effects induced by nearest neighbor Ag surface atoms do play a considerable role, they are responsible for the difference in OH bonding and ORR activity between Pt(Pt_6) sites and Pt($AgPt_5$) sites.

Overall, this study clearly demonstrates the importance of including also more distant neighbors in the description of the adsorption ensemble for modelling the activity of binary surfaces on an atomic scale. On the other hand, it also demonstrates that for a given surface composition the variation in binding energies and thus in catalytic activity induced by different configurations outside the adsorption ensemble may be small and can in many cases be neglected. This is even when considering that the binding energy enters the rate exponentially, leading to a weighting preference for the optimum binding energy. Finally, while focusing here on smooth bimetallic surfaces, a similar approach as described in the above papers is of course also possible for other surfaces and even catalyst nanoparticles with a variety of different active sites. In a more general sense, this also leads to the conclusion that the often used picture of ‘the active site’ is in most cases incorrect. Instead, the reaction is likely to proceed on a number of different active sites, all of which contribute to the overall reaction rates, though by different amounts. Only in cases where the difference in activity between the most active site and other, less active sites is rather large, the reaction will be dominated by a single type of active site. Furthermore, this also means that the reaction may not necessarily be dominated by the most active site. This would be the case, e.g., if the relative number

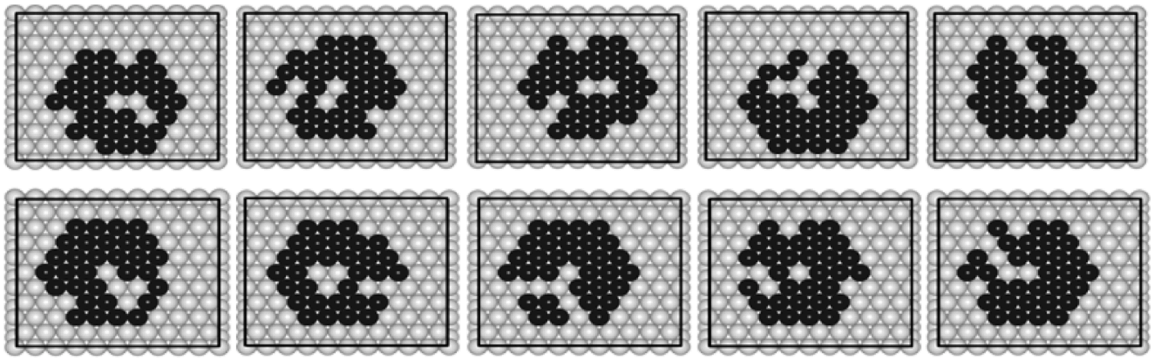

Fig. 12. Examples for different configurations of $Ag_{0.31}Pt_{0.69}$/Pt(111) surfaces with 17 %, 12 %, 18 %, and 53 % of Ag_3, Ag_2Pt, $AgPt_2$, and Pt_3 trimers. Adapted from Ozório et al. [93].

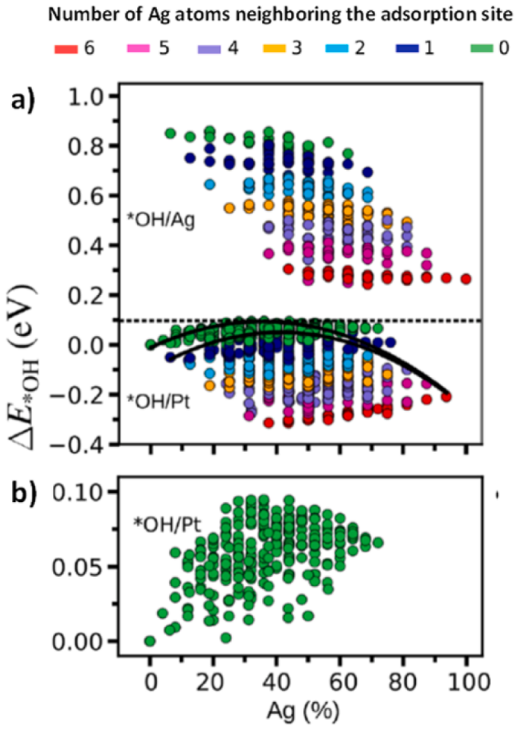

Fig. 13. (a) Distribution of the relative *OH adsorption energies (ΔE_{*OH}) on Ag (top panel) and Pt (bottom panel) surface atoms (different heptamers, see figure) as a function of the Ag surface concentration on the surface slab (energies relative to the OH adsorption energy on Pt(111)). (b) Distribution of relative *OH adsorption energies on Pt in $Pt(Pt_6)$ heptamers, $*OH/Pt(Pt_6)$, plotted on an extended energy scale. Adapted from Ozório et al. [93].

of less active sites is so much larger than that of the most active site that the contribution from the most active site is small compared to the contributions from the other, less active site(s).

Interesting and partly new aspects for future work would, e.g., be the experimental verification of approaches aiming at breaking the scaling relations, using model surfaces with well-defined structural elements [176–180]. Possible candidates would, e.g., be structures where the adsorption energies of reactants and intermediates do not follow a linear scaling law [179], but also reaction mechanisms involving different reaction sites in a sequence of elementary reaction steps. Another fundamental problem refers to possible effects imposed by the surrounding adlayer. In the examples described above, the total rate was calculated as a sum of the rates obtained on different, separated and thus independent adsorption sites. Therefore, microkinetic models including also adlayer mediated interactions between different neighboring active sites would be highly interesting. In electrocatalysis, the consideration of the electrolyte on an inhomogeneous electrode surface on an atomistic level would be highly desirable [150,181]. On the way to a more realistic reaction picture, the inclusion of mesoscopic transport effects on inhomogeneous surfaces on the reaction characteristics would be a consequent next step to extend the current idealized understanding of catalytic reactions. For all of these cases, however, the reproducible generation of structurally well-defined surfaces and the quantitative determination of the different structural elements of interest are a time-consuming pre-condition for mapping out unambiguous structure-reactivity correlations.

4. Summary

In this review on the surface chemistry of bimetallic surfaces and catalysts we have illustrated and demonstrated the following general trends and principles:

1. In many cases, the (initial) structure and surface composition of bimetallic surfaces and catalyst nanoparticles will be determined by kinetic limitations rather than by thermodynamics, and depend on the preparation procedure and conditions. Catalytic reactions at elevated temperatures will drive the structure towards the thermodynamically stable structure.
2. The thermodynamic stability of a bimetallic surface / nanoparticle is given by the (specific) surface energy and the formation energy, where the former describes the stability with respect to the surface structure and faceting, while the latter includes also the composition of the bulk in terms of intermixing or phase separation.
3. Statistical evaluation of extended areas of atomic resolution STM images with chemical contrast can provide detailed, quantitative data on the abundance of different structural elements such as atomic ensembles on bimetallic surfaces, which provide a basis for the quantitative interpretation and modeling of spectroscopic results and kinetic results obtained on these surfaces. On a more qualitative scale, such information can also be obtained from spectroscopy measurements, e.g., via titration with suitable adsorbates.
4. Relevant for the chemical / catalytic properties of bimetallic surfaces and catalysts are the local electronic properties, projected onto the different surface atoms, which are accessible from theory. For a given surface atom, these are predominantly modified by the number, distance and nature of direct neighbors.
5. In addition to the dominant short-range electronic effects, also longer-range strain effects can play a role, which lead to slight variations in the geometrical size and thus in the electronic properties of a given adsorption site / ensemble. These variations are induced, e.g., by the presence of larger or smaller surface atoms outside the adsorption ensemble.

6. Trends in the relative adsorption strength of a given adsorption site or adsorption ensemble, which on a more quantitative scale can be derived from the shifts of the d-band center (d-band model), can be estimated rather well for the dominant late transition metals with a more than half filled d-band in a simple chemical picture, via the principle of constant bond order. This says that depending on the number of bonds from the adsorbing surface atom or adsorption site to neighboring atoms (structural effect) and on their bond strength (electronic effects), the bond to an additional atom/molecule, here the adsorbed species, will be lower or stronger to maintain a constant bond order. For early transition metals with less than half filled d-band, this approach does not work.
7. The overall activity of a bimetallic surface in a given catalytic reaction can be determined rather well in a simple local picture, as the sum over the local activities on the different active sites / ensembles, weighted by the abundance of the number of the respective sites / ensembles on the surface. This also means, that in contrast to the often used picture, there is not only a single type of active site. Instead, in a general approach a variety of active sites with different local activities, which contribute to the total reaction rate based on their local activity and their abundance, have to be considered.

Finally, directions for future work aiming at a further improvement of the mechanistic understanding of adsorption and catalytic reactions on bimetallic surfaces were pointed out.

CRediT authorship contribution statement

R. Jürgen Behm: Writing – review & editing, Writing – original draft, Conceptualization. **Axel Groß:** Writing – review & editing, Writing – original draft, Conceptualization.

Declaration of competing interest

The authors declare that they have no known competing financial interests or personal relationships that could have appeared to influence the work reported in this paper.

Acknowledgement

The graphical abstract is reprinted with permission from Mancera et al. [125], Copyright 2022 American Chemiscal Society.

Data availability

No data was used for the research described in the article.

References

[1] G.-M. Schwab, Alloy catalysts in dehydrogenation, Disc. Faraday Soc. 8 (1950) 166–171.
[2] D.A. Dowden, P.W. Reynolds, Some reactions over alloy catalysts, Disc. Faraday Soc. 8 (1950) 184–190.
[3] J.H. Sinfelt, Catalysis by alloys and bimetallic clusters, Acc. Chem. Res. 10 (1977) 15–20.
[4] W.M.H. Sachtler, R.A. van Santen, Surface composition and selectivity of binary alloys, Adv. Catal. 26 (1977) 69–119.
[5] V. Ponec, Alloy catalysts: the concept, Appl. Catal. A 222 (2001) 31–45.
[6] J.H. Sinfelt, Role of Surface Science in Catalysis, Surf. Sci. 500 (2002) 923–946.
[7] Y. Soma-Noto, W.M.H. Sachtler, Infrared spectra of carbon monoxide adsorbed on supported palladium and palladium-silver alloys, J. Catal. 32 (1974) 315–324.
[8] V. Ponec, Surface composition and catalysis on alloys, Surf. Sci. 80 (1979) 352–366.
[9] W.M.H. Sachtler, The second rideal lecture. what makes a catalyst selective ? Faraday Discuss. Chem. Soc. 72 (1981) 7–31.
[10] J.W.A. Sachtler, G.A. Somorjai, Influence of ensemble size on CO chemisorption and catalytic N-hexane conversion by Au-Pt(111) bimetallic single-crystal surfaces, J. Catal. 81 (1983) 77–94.
[11] W.M.H. Sachtler, P. van der Plank, The role of individual surface atoms in chemisorption and catalysis by nickel-copper alloys, Surf. Sci. 18 (1969) 62–79.
[12] V. Ponec, W.M.H. Sachtler, The reactions between cyclopentane and deuterium on nickel and nickel-copper alloys, J. Catal. 24 (1972) 250–261.
[13] Y.L. Lam, J. Criado, M. Boudart, Enhancement by inactive gold of the rate of the H_2-O_2reaction on active palladium: a ligand effect, Nouv. J. Chim. 1 (1977) 461–466.
[14] J.A. Rodriguez, Physical and chemical properties of bimetallic surfaces, Surf. Sci. Rep. 24 (1996) 223–288.
[15] M. Mavrikakis, B. Hammer, J.K. Nørskov, Effect of strain on the reactivity of metal surfaces, Phys. Rev. Lett. 81 (1998) 2819–2822.
[16] B. Hammer, J.K. Nørskov, Theoretical surface science and catalysis-calculations and concepts, Adv. Catal. 45 (2000) 71–129.
[17] A. Groß, Reactivity of bimetallic systems studied from first principles, Top. Catal. 37 (2006) 29–40.
[18] A. Groß, Tailoring the reactivity of bimetallic overlayer and surface alloy systems, J. Phys. Condens. Matter 21 (2009) 084205.
[19] J.T. Yates, C.H.F. Peden, D.W. Goodman, Copper site blocking of hydrogen chemisorption on ruthenium, J. Catal. 94 (1985) 576–580.
[20] R.G. Windham, B.E. Koel, M.T. Paffett, Studies of the ensemble size requirements for ethylene adsorption and decomposition on platinum(111): ethylene and bismuth coadsorption, Langmuir 4 (1988) 1113–1118.
[21] C. Xu, B.E. Koel, Probing the Modifier Precursor State: adsorption of CO on Sn/Pt (111) Surface Alloys, Surf. Sci. 304 (1994) L505–L511.
[22] D.A. Dowden, 56. Heterogeneous catalysis. Part I. Theoretical basis, J. Chem. Soc. 1950 (1950) 242–265.
[23] J.H. Sinfelt, Catalytic hydrogenolysis over supported metals, Catal. Rev. 3 (1970) 175–205.
[24] J.H. Sinfelt, Y.L. Lam, J.A. Cusamano, A.E. Barnett, Nature of ruthenium-copper catalysts, J. Catal. 42 (1976) 227–235.
[25] J.H. Sinfelt, J.L. Carter, D.J.C. Yates, Catalytic hydrogenolysis and dehydrogenation over copper-nickel alloys, J. Catal. 24 (1972) 283–296.
[26] C.T. Campbell, Bimetallic surface chemistry, Annu. Rev. Phys. Chem. 41 (1990) 775–837.
[27] J.A. Rodriguez, D.W. Goodman, The nature of the metal-metal bond in bimetallic surfaces, Science 257 (1992) 897–903.
[28] G.R. Rao, Chemistry of bimetallic surfaces, Curr. Sci. 75 901–910.
[29] K. Christmann, G. Ertl, H. Shimizu, The Growth and structure of copper films on (0001) ruthenium surfaces, Thin Solid Films 57 (1979) 247–252.
[30] K. Christmann, G. Ertl, H. Shimizu, Model studies on bimetallic Cu/Ru catalysts I. Cu on Ru(0001), J. Catal. 61 (1980) 397–411.
[31] J.C. Vickerman, K. Christmann, Model studies on bimetallic Cu/Ru catalysts IV. Adsorption of $D_2$and Co-adsorption of CO and D_2, Surf. Sci. 120 (1982) 1–18.
[32] D.W. Goodman, J.T. Yates, C.H.F. Peden, The reaction of atomic copper with chemisorbed hydrogen on ruthenium, Surf. Sci. 164 (1985) 417–424.
[33] D.W. Goodman, C.H.F. Peden, Hydrogen spillover from ruthenium to copper in Cu/Ru catalysts: a potential source of error in active metal titration, J. Catal. 95 (1985) 321–324.
[34] M.H. Tsai, J.W. Yeh, High-entropy alloys: a critical review, Mater. Res. Lett. 2 (2014) 107–123.
[35] I. Song, Surface alloys in nanochemistry: catalysis and synthesis, New J. Chem. 44 (2020) 18525–18529.
[36] J. Greeley, M. Mavrikakis, Near-surface alloys for hydrogen fuel cell applications, Catal. Today 111 (2006) 52–58.
[37] J. Tersoff, F.K. LeGoues, Competing relaxation mechanisms in strained layers, Phys. Rev. Lett. 72 (1994) 3570–3573.
[38] J.H. van der Merwe, D.L. Tönsing, P.M. Stoop, Role of misfit strain and proximity in epigrowth modes I. Strong epilayer-substrate interaction, Surf. Sci. 312 (1994) 387–398.
[39] H. Brune, H. Röder, C. Boragno, K. Kern, Strain relief at hexagonal-close-packed interfaces, Phys. Rev. B 49 (1994) 2997–3000.
[40] C. Günther, J. Vrijmoeth, R.Q. Hwang, R.J. Behm, Strain relaxation in hexagonally close-packed metal-metal interfaces, Phys. Rev. Lett. 74 (1995) 754–757.
[41] C. Ammer, K. Meinel, H. Wolter, A. Beckmann, H. Neddermeyer, High-resolution LEED analysis of strained Cu layers on Ru(0001), Surf. Sci. 375 (1997) 302–314.
[42] E. Bauer, Phänomenologische Theorie der Kristallabscheidung an Oberflächen II, Z. Krist. 110 (1958) 395–431.
[43] E. Bauer, Phänomenologische Theorie der Kristallabscheidung an Oberflächen I, Z. Krist. 110 (1958) 372–394.
[44] J.H. van der Merwe, Interplay between misfit strain relief and stranski-krastanov growth in Fcc (111)/Bcc (110) ultrathin film epitaxy. Part 1. analytical approach, Surf. Sci. 449 (2000) 151–166.
[45] In (Ed.), The Chemical Physics of Solid Surfaces, Surface Alloys and Alloy Surfaces, Woodruff (Ed.), Elsevier, Amsterdam, 2002.
[46] G. Ertl, J. Küppers, Low Energy Electrons and Surface Chemistry, Wiley-VCH, Weinheim, 1985, 2. ed.
[47] H. Zajonz, D. Gibbs, A.P. Baddorf, V. Jahns, D.M. Zehner, Structure and growth of strained Cu films on Ru(0001), Surf. Sci. 447 (2000) L141–L146.
[48] V.M. Hallmark, S. Chiang, J.F. Robolt, J.D. Swalen, R.J. Wilson, Observation of atomic corrugation on Au(111) by STM, Phys. Rev. Lett. 59 (1987) 2879–2882.
[49] C. Wöll, S. Chiang, R.J. Wilson, P.H. Lippel, Determination of atom positions at stacking-fault dislocations on Au(111) by STM, Phys. Rev. B 39 (1989) 7988–7991.
[50] J. Wintterlin, J. Wiechers, H. Brune, T. Gritsch, H. Höfer, R.J. Behm, Atomic-resolution imaging of close-packed metal surfaces by STM, Phys. Rev. Lett. 62 (1989) 59–62.

[51] M. Schmid, H. Stadler, P. Varga, Direct observation of surface chemical order by scanning tunneling microscopy, Phys. Rev. Lett. 70 (1993) 1441–1444.
[52] P.T. Wouda, B.E. Nieuwenhuys, M. Schmid, P. Varga, Chemically resolved STM on a PtRh(100) surface, Surf. Sci. 359 (1996) 17–22.
[53] F. Buatier de Mongeot, M. Scherer, B. Gleich, E. Kopatzki, R.J. Behm, CO adsorption and oxidation on bimetallic Pt/Ru(0001) surfaces - A combined STM and TPD/TPR study, Surf. Sci. 411 (1998) 249–262.
[54] J.V. Barth, H. Brune, G. Ertl, R.J. Behm, Scanning tunneling microscopy observations on the reconstructed Au(111) surface: atomic structure, long-range superstructure, rotational domains, and surface defects, Phys. Rev. B 42 (1990) 9307.
[55] A. Bergbreiter, Präparation und Charakterisierung bimetllischer AuPt Oberflächen: Atomare Nanostrukturen und ihre Chemischen Eigenschaften, Ulm University, 2005. Diploma Thesis.
[56] H.E. Hoster, A. Bergbreiter, P. Erne, T. Hager, H. Rauscher, R.J. Behm, Atomic distribution in well-defined Pt_xRu_{1-x}/Ru(0001) monolayer surface alloys, Phys. Chem. Chem. Phys. 10 (2008) 3812–3823.
[57] R. Rötter, Atomverteilung in zweidimensionalen Pt_xAg_{1-x}Legierungen auf Pt (111), Ulm University, 2009. IDiploma Thesis.
[58] A.K. Engstfeld, H.E. Hoster, R.J. Behm, Formation, atomic distribution and mixing energy in two-dimensional Ag_xPd_{1-x}surface alloys on Pd(111), Phys. Chem. Chem. Phys. 14 (2012) 10754–10761.
[59] M.S. Chen, K. Luo, T. Wei, Z. Yan, D. Kumar, C.W. Yi, D.W. Goodman, The nature of the active sites for vinyl acetate synthesis over Pd-Au, Catal. Today 117 (2006) 37–45.
[60] Y. Ma, J. Bansmann, T. Diemant, R.J. Behm, Formation, stability and CO adsorption properties of PdAg/Pd(111) surface alloys, Surf. Sci. 603 (2009) 1046–1054.
[61] Y. Ma, T. Diemant, J. Bansmann, R.J. Behm, The interaction of CO with PdAg/Pd (111) surface alloys - A case study of ensemble effects on a bimetallic surface, Phys. Chem. Chem. Phys. 13 (2011) 10741–10754.
[62] U. Bauer, F. Späth, F. Düll, P. Bachmann, J. Steinhauer, H.P. Steinrück, C. Papp, Reactivity of CO and C_2H_4 on bimetallic Pt_xAg_{1-x}/Pt(111) surface alloys investigated by high-resolution X-ray photoelectron spectroscopy, ChemPhysChem 19 (2018) 1432–1440.
[63] L.P. Nielsen, I. Stensgaard, F. Besenbacher, E. Laegsgaard, Combined STM and RBS investigation of the nucleation and growth of Au on Ni(110): alloying and dealloying, Surf. Rev. Lett. 3 (1996) 1713–1719.
[64] K.J. Andersson, F. Calle-Vallejo, J. Rossmeisl, I. Chorkendorff, Adsorption-driven surface segregation of the less reactive alloy component, J. Am. Chem. Soc. 131 (2009) 2404–2407.
[65] C.A. Menning, J.G. Chen, General trend for adsorbate-induced segregation of subsurface metal atoms in bimetallic surfaces, J. Chem. Phys. 130 (2009) 174709.
[66] T.P. Moffat, F.R.F. Fan, A.J. Bard, Electrochemical and STM study of dealloying of Cu_3Au, J, Electrochem. Soc. 138 (1991) 3223–3235.
[67] S. Beckord, A.K. Engstfeld, S. Brimaud, R.J. Behm, Electrochemical characterization and stability of Ag_xPt_{1-x}/Pt(111) surface alloys, J. Phys. Chem. C 120 (2016) 16179–16190.
[68] S. Beckord, S. Brimaud, R.J. Behm, Stability and ORR performance of a well-defined bimetallic $Ag_{70}Pt_{30}$/Pt(111) monolayer surface alloy electrode - probing the de-alloying at an atomic scale, Electrochim. Acta 259 (2018) 762–771.
[69] M.A. van Spronsen, K. Daunmu, C.R. O'Connor, T. Egle, H. Kersell, J. Oliver-Meseguer, M.B. Salmeron, R.J. Madix, P. Sautet, C.M. Friend, Dynamics of Surface Alloys: rearrangement of Pd/Ag(111) induced by CO and O_2, J. Phys. Chem. C 123 (2019) 8312–8323.
[70] D.A. Patel, P.L. Kress, L.A. Cramer, A.M. Larson, E.C. Sykes, Elucidating the composition of PtAg surface alloys with atomic-scale imaging and spectroscopy, J. Chem. Phys. 151 (2019) 164705.
[71] J.S. Lim, J. Vandermause, M.A. van Spronsen, A. Musaelian, Y. Xie, L. Sun, C. R. O'Connor, T. Egle, N. Molinari, J. Florian, K. Duanmu, R.J. Madix, P. Sautet, C. M. Friend, B. Kozinsky, Evolution of metastable structures at bimetallic surfaces from microscopy and machine-learning molecular dynamics, J. Am. Chem. Soc. 142 (2020) 15907–15916.
[72] C.R. O'Connor, K. Duanmu, D.A. Patel, E. Muramoto, M.A. van Spronsen, D. Stacchiola, E.C. Sykes, P. Sautet, R.J. Madix, C.M. Friend, Facilitating hydrogen atom migration via a dense phase on palladium islands to a surrounding silver surface, Proc. Natl. Acad. Sci. 117 (2020) 22657–22664.
[73] B.S.A. Gedara, M. Muir, A. Islam, D. Liu, M. Trenary, Room temperature migration of Ag atoms to cover Pd islands on Ag(111), J. Chem. Phys. C 125 (2021) 27828–27836.
[74] B.S.A. Gedara, M. Trenary, Stability of Pd islands on Ag(111) and Au(111), J. Chem. Phys. C 127 (2023) 516–522.
[75] T. Bligaard, J.K. Nørskov, S. Dahl, J. Matthiesen, C.H. Christensen, J. Sehested, The Brønsted-Evans-Polanyi relation and the volcano curve in heterogeneous catalysis, J. Catal. 224 (2004) 206–217.
[76] J.M. Guglielmacci, M. Gillet, Charactrisation par spectrometrie Auger Et De capage ionique des modes de croissance Et De L'Interface dans le couple Ag-Pd, Thin Solid Films 68 (1980) 407–416.
[77] J. Rodriguez, C.M. Truong, D.W. Goodman, FT-IRAS studies of CO adsorbed on Ag/Pt(111): anomalous behavior of vibrational cross-sections, Surf. Sci. 271 (1992) L331–L337.
[78] B. Eisenhut, J. Stober, G. Rangelov, T. Fauster, Growth and structure of Ag on Pd (111) studied by photoelectron forward scattering using a two-dimensional display-type analyzer, Phys. Rev. B 47 (1993) 12980–12983.
[79] R. Fischer, S. Schuppler, N. Fischer, T. Fauster, W. Steinmann, Image states and local work function for Ag/Pd(111), Phys. Rev. Lett. 70 (1993) 654–657.
[80] V.M. Trontl, M. Pletikosic, M. Milun, P. Pervan, D. Lazic, R. Sokcevic, R. Brako, Experimental and ab initio study of the structural and electronic properties of subnanometer thick Ag film on Pd (111), Phys. Rev. B 72 (2008) 235418–235418-11.
[81] P.W. Davies, M.A. Quinlan, G.A. Somorjai, The growth and chemisorptive properties of ag and au monolayers on platinum single crystal surfaces: an AES, TDS and LEED Study, Surf. Sci. 121 (1982) 290–302.
[82] G. Rangelov, T. Fauster, U. Strüber, J. Küppers, Stacking of Ag Layers on Pt(111), Surf. Sci. 331-333 (1995) 948–951.
[83] D. Mahlberg, A. Gross, Vacancy assisted diffusion on single-atom surface alloys, ChemPhysChem 22 (2021) 29–39.
[84] D. Mahlberg, S. Sakong, A. Groß, Structure of PtRu/Ru(0001) and AgPd/Pd(111) surface alloys: a kinetic monte carlo study, Chem Phys 555 (2022) 111428.
[85] H. Röder, R. Schuster, H. Brune, K. Kern, Monolayer-confined mixing at the Ag-Pt (111) interface, Phys. Rev. Lett. 71 (1993) 2086–2089.
[86] U. Strüber, J. Küppers, Spectroscopic confirmation of STM Derived Ag/Pt mixing in annealed Ag submonolayers at Pt(111) surfaces, Surf. Sci. 294 (1993) L924–L928.
[87] T. Härtel, U. Strüber, J. Küppers, Growth and properties of thin Ag films on Pt (111) Surfaces, Thin Solid Films 229 (1993) 163–170.
[88] J.S. Tsay, Y.D. Yao, C.S. Shern, Dynamic study of a surface-confined alloy in ultrathin Ag/Pt(111) film, Phys. Rev. B 58 (1998) 3609–3612.
[89] M. Jankowski, H. Wormeester, H.J.W. Zandvliet, B. Poelsema, Temperature dependent formation and evolution of the interfacial dislocation network of Ag/Pt(111), Phys. Rev. B 89 (2014) 235402.
[90] M. Jankowski, E. van Vroonhoven, H. Wormeester, H.J.W. Zandvliet, B. Poelsema, Alloying, dealloying, and reentrant alloying in (Sub)monolayer growth of Ag on Pt(111), J. Chem. Phys. C 121 (2017) 8353–8363.
[91] M.T. Paffet, C.T. Campbell, T.N. Taylor, Surface chemical properties of Ag/Pt (111): comparisons between electrochemistry and surface science, Langmuir 1 (1985) 741–747.
[92] J.M. Cowley, X-ray measurement of order in single crystals of Cu_2Au, J. Appl. Phys. 21 (1950) 24–30.
[93] M.S. Ozório, M.F. Nygaard, A.S. Petersen, R.J. Behm, J. Rossmeisl, Self-induced long-range surface strain improves oxygen reduction reaction, J. Catal. 433 (2024) 115484.
[94] F. Maroun, F. Ozanam, O.M. Magnussen, R.J. Behm, The role of atomic ensembles in the reactivity of bimetallic electrocatalysts, Science 293 (2001) 1811–1814.
[95] M. Muir, M. Trenary, Adsorption of CO to characterize the structure of a Pd/Ag (111) single-atom alloy surface, J. Chem. Phys. C 124 (2020) 14722–14729.
[96] D.A. Dowden, Research 1 (1948) 239.
[97] D.A. Dowden, P.W. Reynolds, Heterogeneous catalysis, Nature 164 (1949) 50–52.
[98] P.W. Reynolds, Heterogeneous catalysis. Part II. Hydrogenation by binary alloys, J. Chem. Soc. (Resumed) 1950 (1950) 265–271.
[99] A. Couper, D.D. Eley, Parahydrogen catalysis by transition metals, Nature 164 (1949) 578–579.
[100] A. Ozaki, K. Aika, Catalytic activation of dinitrogen, in: J.R. Anderson, M. Boudart (Eds.), Catalysis Science and Technology 1, Springer, Verlag, Berlin, 1981.
[101] S. Trasatti, Work function, electronegativity, and electrochemical behaviour of metals: III. Electrolytic hydrogen evolution in acid solutions, J. Electroanal. Chem. 39 (1972) 163–184.
[102] C. Kittel, Introduction to Solid State Physics, 9th edition, Wiley & Sons, 2018.
[103] D.M. Newns, Self-consistent model of hydrogen chemisorption, Phys. Rev. 178 (1969) 1123–1135.
[104] P.J. Feibelman, D.R. Hamann, Electronic structure of a "poisoned" transition-metal surface, Phys. Rev. Lett. 52 (1984) 61–64.
[105] J. Harris, S. Andersson, H_2 dissociation at metal surfaces, Phys. Rev. Lett. 55 (1985) 1583–1586.
[106] R. Hoffmann, A chemical and theoretical way to look at bonding on surfaces, Rev. Mod. Phys. 60 (1988) 601–628.
[107] A. Groß, Adsorption at nanostructured surfaces from first principles, J. Comput. Theor. Nanosci. 5 (2008) 894–922.
[108] B. Hammer, J.K. Nørskov, Electronic factors determining the reactivity of metal surfaces, Surf. Sci. 343 (1995) 211–220.
[109] V. Pallassana, M. Neurock, L.B. Hansen, B. Hammer, J.K. Nørskov, Theoretical analysis of hydrogen chemisorption on Pd(111), Re(0001) and Pd_{ML}/Re(0001), Re_{ML}/Pd(111) pseudomorphic overlayers, Phys. Rev. B 60 (1999) 6146–6154.
[110] A. Vojvodic, J.K. Nørskov, F. Abild-Pedersen, Electronic structure effects in transition metal surface chemistry, Top. Catal. 57 (2014) 25–32.
[111] H. Xin, A. Vojvodic, J. Voss, J.K. Nørskov, F. Abild-Pedersen, Effects of *D*-band shape on the surface reactivity of transition-metal alloys, Phys. Rev. B 89 (2014) 115114.
[112] A. Groß, Theoretical Surface Science - A Microscopic Perspective, 2nd Ed., Springer, Berlin, 2009.
[113] H. Hopster, H. Ibach, Adsorption of CO on Pt(111) and Pt(6(111) x (111) studied by high resolution electron energy loss spectroscopy and thermal desorption spectroscopy, Surf. Sci. 77 (1978) 109–117.
[114] M.R. McClellan, J.L. Gland, F.R. McFeeley, Carbon monoxide adsorption on the kinked Pt(321) surface, Surf. Sci. 112 (1981) 63–77.
[115] B.E. Hayden, K. Kretzschmar, A.M. Bradshaw, R.G. Greenler, An infrared study of the adsorption of CO on a stepped platinum surface, Surf. Sci. 149 (1985) 394–406.
[116] J.T. Yates, Surface chemistry at metallic step defect sites, J. Vac. Sci. Technol. A 13 (3) (1995) 1359–1367.
[117] F. Garcia-Martinez, E. Turco, F. Schiller, J.E. Ortega, CO and O_2 interaction with kinked Pt surfaces, ACS Catal 14 (2024) 6319–6327.

[118] B. Hammer, O.H. Nielsen, J.K. Nørskov, Structure sensitivity in adsorption: CO interaction with stepped and reconstructed Pt surfaces, Catal. Lett. 46 (1997) 31–35.
[119] I. Mayer, Charge, bond order and valence in the ab initio SCF theory, Chem. Phys. Lett. 97 (1983) 270–274.
[120] S. Schnur, A. Groß, Strain and coordination effects in the adsorption properties of early transition metals: a density-functional theory study, Phys. Rev. B 81 (2010) 033402–033402-3.
[121] G. Wulff, XXV. Zur Frage der Geschwindigkeit des Wachsthums und der Auflösung der Kristallflächen, Z. Krist. 34 (1901) 449–530.
[122] S. Sakong, A. Groß, R.J. Behm, Surface, interface, compression and formation energies of bimetallic Ag/Pt(111) and Ag/Pd(111) surfaces from first-principles, J. Chem. Phys. C 128 (2024) 13558.
[123] A.P. Farkas, T. Diemant, J. Bansmann, R.J. Behm, The adsorption of oxygen and coadsorption of CO and oxygen on PdAg/Pd(111) surface alloys, ChemPhysChem 13 (2012) 3516–3525.
[124] L.A. Mancera, R.J. Behm, A. Groß, Structure and local reactivity of PdAg/Pd(111) surface alloys, Phys. Chem. Chem. Phys. 15 (2013) 1497–1508.
[125] L.A. Mancera, T. Diemant, A. Groß, R.J. Behm, Molecular and dissociative hydrogen adsorption on bimetallic PdAg/Pd(111) surface alloys: a combined experimental and theoretical study, J. Phys. Chem. C 126 (2022) 3060–3077.
[126] T. Diemant, K.M. Schüttler, R.J. Behm, Ag on Pt(111): changes in electronic and CO adsorption properties upon PtAg/Pt(111) monolayer surface alloy formation, ChemPhysChem 16 (2015) 2943–2952.
[127] K.M. Schüttler, L.A. Mancera, T. Diemant, A. Groß, R.J. Behm, Interaction of CO with Pt_xAg_{1-x}/Pt(111) surface alloys: more than dilution by Ag atoms, Surf. Sci. 650 (2016) 237–254.
[128] L.A. Mancera, A. Groß, R.J. Behm, Stability, electronic properties and CO adsorption properties of bimetallic PtAg/Pt(111) surfaces, Phys. Chem. Chem. Phys. 26 (2024) 18435–18448.
[129] S.V. Barabash, V. Blum, S. Müller, A. Zunger, Prediction of unusual stable ordered structures of Au-Pd alloys via first-principles cluster expansion, Phys. Rev. B 74 (2006) 035108.
[130] T. Egle, C.R. O'Connor, C.M. Friend, Regeneration of active surface alloys during cyclic oxidation and reduction: oxidation of H_2on Pd/Ag(111), J. Phys. Chem. Lett. 12 (2021) 6752–6759.
[131] M. Jankowski, H. Wormeester, H.J.W. Zandvliet, B. Poelsema, Desorption of oxygen from alloyed Ag/Pt (111), J. Chem. Phys. 140 (2014) 234705.
[132] M. Hua, X. Tian, S. Li, A. Shao, X. Lin, Theoretical design of platinum-silver single atom alloy catalysts with CO adsorbate-induced surface structures, Phys. Chem. Chem. Phys. 24 (2022) 19488–19501.
[133] G.A. Kok, A. Noordermeer, B.E. Nieuwenhuys, Effects of alloying on the adsorption of CO on palladium: a comparison of the behaviour of PdAg(111), PdCu(111) and Pd(111) surface, Surf. Sci. 152-153 (1985) 505–512.
[134] A. Noordermeer, G.A. Kok, B.E. Nieuwenhuys, A comparative study of the behaviour of the PdAg(111) and Pd(111) surfaces towards the interaction with hydrogen and carbon monoxide, Surf. Sci. 165 (1986) 375–392.
[135] I.H. Svenum, J.A. Herron, M. Mavrikakis, H.J. Venvik, $Pd_3Ag(111)$ as a model system for hydrogen separation membranes: combined effects of CO adsorption and surface termination on the activation of molecular hydrogen, Top. Catal. 63 (2020) 750–761.
[136] W. Hansen, M. Bertolo, K. Jacobi, Physisorption of CO on Ag(111): investigation of the monolayer and the multilayer through HREELS, ARUPS, and TDS, Surf. Sci. 253 (1991) 1–12.
[137] O. Björneholm, A. Nilsson, H. Tillborg, P. Bennich, A. Sandell, B. Hernnäs, C. Puglia, N. Martensson, Overlayer structure from adsorbate and substrate core level binding energy shifts: CO, $CCH_3$and O on Pt(111), Surf. Sci. 315 (1994) L983–L989.
[138] P.J. Feibelman, B. Hammer, J.K. Nørskov, F. Wagner, M. Scheffler, R. Stumpf, R. Watwe, J. Dumesic, The CO/Pt(111) Puzzle, J. Phys. Chem. B 105 (2001) 4018–4025.
[139] S.Y. Chin, C.T. Willimas, M.D. Amiridis, FTIR studies of CO adsorption on Al_2O_3- and SiO_2-supported Ru catalysts, J. Phys. Chem. B 110 (2006) 871–882.
[140] B.T. Loveless, C. Buda, M. Neurock, E. Iglesia, CO chemisorption and dissociation at high coverages during CO hydrogenation on Ru catalysts, J. Am. Chem. Soc. 135 (2013) 6107–6121.
[141] Y. Yan, Q. Wang, C. Jiang, Y. Yao, D. Lu, J. Zheng, Y. Dai, H. Wang, Y. Yang, Ru/Al_2O_3catalyzed CO_2hydrogenation: oxygen-exchange on metal-support interfaces, J. Catal. 367 (2018) 194–205.
[142] S.C. Tsang, N. Cailuo, W. Oduro, A.T.S. Kong, L. Clifton, K.M.K. Yu, B. Thiebaut, J. Cookson, P. Bishop, Engineering preformed cobalt-doped platinum nanocatalysts for ultraselective hydrogenation, ACS Nano 2 (2008) 2547–2553.
[143] W.O. Oduro, N. Cailuo, K.M. Yu, H. Yang, S.C. Tsang, Geometric and electronic effects on hydrogenation of cinnamaldehyde over unsupported pt-based nanocrystals, Phys. Chem. Chem. Phys. 13 (2011) 2590–2602.
[144] T. Gießel, O. Schaff, C.J. Hirschmugl, V. Fernandez, K.M. Schindler, A. Theobald, S. Bao, R. Lindsay, W. Berndt, A.M. Bradshaw, C. Baddeley, A.F. Lee, R. M. Lambert, D.P. Woodruff, A photoelectron diffraction study of ordered structures in the chemisorption system Pd(111)-CO, Surf. Sci. 406 (1998) 90–102.
[145] S. Surnev, M. Sock, M.G. Ramsey, F.P. Netzer, M. Wiklund, M. Borg, J. N. Andersen, CO adsorption on Pd(111): a high-resolution core level photoemission and electron energy loss spectroscopy study, Surf. Sci. 470 (2000) 171–185.
[146] M. Ruff, N. Takehiro, P. Liu, J.K. Nørskov, R.J. Behm, Size-specific chemistry on bimetallic surfaces: a combined experimental and theoretical study, ChemPhysChem 8 (2007) 2068–2071.
[147] R.J. Gorte, L.D. Schmidt, Interactions between NO and CO on Pt(111), Surf. Sci. 111 (1981) 260–278.
[148] H. Steininger, S. Lehwald, H. Ibach, On the adsorption of CO on Pt(111), Surf. Sci. 123 (1982) 264–282.
[149] P.T. Wouda, M. Schmid, B.E. Nieuwenhuys, P. Varga, STM study of the (111) and (100) surfaces of PdAg, Surf. Sci. 417 (1998) 292–300.
[150] A. Groß, S. Sakong, Ab initio simulations of water/metal interfaces, Chem. Rev. 122 (2022) 10746–10776.
[151] N. Takehiro, P. Liu, A. Bergbreiter, J.K. Nørskov, R.J. Behm, Hydrogen adsorption on bimetallic PdAu(111) surface alloys: minimum adsorption ensemble, ligand and ensemble effects, and ensemble confinement, Phys. Chem. Chem. Phys. 16 (2014) 23930–23942.
[152] I. Langmuir, PartII."Heterogeneous reactions" - chemical reactions on surfaces, Trans. Faraday Soc. 17 (1922) 607–620.
[153] D.D. Eley, Mechanisms of hydrogen catalysis, Q. Rev. Chem. Soc. 1948 (1948) 209–225.
[154] P. Mars, D.W. van Krevelen, Oxidations carried out by means of vanadium oxide catalysts, Chem. Eng. Sci. 3 (1954) 41–59. Supplement.
[155] R. Prins, Eley-Rideal, the other mechanism, Top. Catal. 61 (2018) 714–721.
[156] T. Engel, G. Ertl, Elementary steps in the catalytic oxidation of carbon monoxide on platinum metals, Adv. Catal. 28 (1979) 2–79.
[157] D. Widmann, R.J. Behm, Active oxygen on a Au/TiO_2 catalyst - formation, stability and CO oxidation activity, Angew. Chem. Int. Ed. 50 (2011) 10241–10245.
[158] D. Widmann, R.J. Behm, Activation of molecular oxygen and the nature of the active oxygen species for CO oxidation on oxide supported au catalysts, Acc. Chem. Res. 47 (2014) 740–749.
[159] R.H. Griffith, Advances in Catalysis, 1st ed., Academic Press, New York, 1948. W. G. Frankenburg, V. I. Komarewsky, and E. K. Rideal, Eds.
[160] M. Watanabe, S. Motoo, Electrocatalysis by adatoms: part II. Enhancement of the oxidation of methanol on platinum by ruthenium adatoms, J. Electroanal. Chem. 60 (1975) 267–273.
[161] M. Watanabe, S. Motoo, Electrocatalysis by adatoms Part III. Enhancement of the oxidation of carbon monoxid on platinum by ruthenium adatoms, J. Electroanal. Chem. 60 (1975) 275–283.
[162] A. Schlapka, M. Lischka, A. Groß, U. Käsberger, P. Jakob, Surface strain versus substrate interaction in heteroepitaxial metal layers: pt on Ru(0001), Phys. Rev. Lett. 91 (2003), 016101-1-016101-4.
[163] A. Baz, A. Holewinski, Understanding the interplay of bifunctional and electronic effects: microkinetic modeling of the CO electro-oxidation reaction, J. Catal. 384 (2020) 1–13.
[164] P. Sabatier, Hydrogénations et déshydrogénations par catalyse, Ber. Dtsch. Chem. Ges. 44 (1911) 1984–2001.
[165] P. Sabatier, La Catalyse en Chimie Organique, Librairie Polytechnique Béranger, Paris, 1913.
[166] M. Che, Nobel prize in chemistry 1912 to sabatier: organic chemistry or catalysis? Catal. Today 218-219 (2013) 162–171.
[167] J.H. Sinfelt, Catalytic hydrogenolysis on metals, Catal. Lett. 9 (1991) 159–172.
[168] A.J. Medford, A. Vojvodic, J.S. Hummelshøj, J. Voss, F. Abild-Pedersen, F. Studt, T. Bligaard, A. Nilsson, J.K. Nørskov, From the Sabatier principle to a predictive theory of transition-metal heterogeneous catalysis, J. Catal. 328 (2015) 36–42.
[169] S. Brimaud, A.K. Engstfeld, O.B. Alves, H.E. Hoster, R.J. Behm, Oxygen reduction on structurally well-defined, bimetallic PtRu surfaces: monolayer Pt_xRu_{1-x}/Ru (0001) surface alloys versus Pt film covered Ru(0001), Top. Catal. 57 (2014) 222–235.
[170] S. Brimaud, A.K. Engstfeld, O.B. Alves, R.J. Behm, Structure-reactivity correlation in the oxygen reduction reaction: activity of structurally well defined Au_xPt_{1-x}/Pt (111) monolayer surface alloys, J. Electroanal. Chem. 716 (2014) 71–79.
[171] S. Beckord, S. Brimaud, R.J. Behm, The performance of structurally well-defined Ag_xPt_{1-x}/Pt(111) surface alloys in the oxygen reduction reaction-an atomic-scale picture, J. Electroanal. Chem. 819 (2018) 401–409.
[172] J.K. Nørskov, J. Rossmeisl, A. Logadottir, L. Lindqvist, J.R. Kitchin, T. Bligaard, H. Jónsson, Origin of the overpotential for oxygen reduction at a fuel-cell cathode, J. Phys. Chem. B 108 (2004) 17886–17892.
[173] A. Damjanovic, V. Brusic, Electrode kinetics of oxygen reduction on oxide-free platinum electrodes, Electrochim. Acta 12 (1967) 615–628.
[174] A. Holewinski, L. Sunjic, Elementary mechanisms in electrocatalysis: revisiting the ORR tafel slope, J. Electrochem. Soc. 159 (2012) H864–H870.
[175] J.K. Pedersen, T.A.A. Batchelor, D. Yan, L.E. Skjegstad, J. Rossmeisl, Surface electrocatalysis on high-entropy alloys, Curr. Opin. Electrochem. 26 (2021) 100651.
[176] M. Andersen, S.V. Levchenko, M. Scheffler, K. Reuter, Beyond scaling relations for the description of catalytic materials, ACS Catal. 9 (2019) 2752–2759.
[177] W. Huang, P.M. Attia, H. Wang, S.E. Renfrew, N. Jin, S. Das, Z. Zhang, D.T. Boyle, Y. Li, M.Z. Bazant, B.D. McCloskey, W.C. Chueh, Y. Cui, Evolution of the solid-electrolyte interphase on carbonaceous anodes visualized by atomic-resolution cryogenic electron microscopy, Nano Lett. 19 (2019) 5140–5148.
[178] J. Masa, W. Schuhmann, Breaking scaling relations in electrocatalysis, J. Solid State Electrochem. 24 (2020) 2181–2182.
[179] S. Vijay, G. Kastlunger, K. Chan, J.K. Nørskov, Limits to scaling relations between adsorption energies? J. Chem. Phys. 156 (2022) 231102.
[180] R. Cepitis, V. Ivanistsev, J. Rossmeisl, N. Kongi, Bypassing the scaling relations in oxygen electrocatalysis with geometry-adaptive catalysts, Catal. Sci. Technol. 14 (2024) 2105–2113.
[181] A. Groß, Challenges in the modeling of elementary steps in electrocatalysis, Curr. Opin. Electrochem. 37 (2023) 101170.